Planar and orthotropic closures for orientation tensors in fiber suspension flow models

Dmitri Kuzmin

Institute of Applied Mathematics (LS III), TU Dortmund University, Vogelpothsweg 87, D-44227 Dortmund, Germany

Abstract

This paper presents a bottom-up approach to derivation of orientation tensor closures for fiber suspension flow models. To begin with, we consider polynomial approximations based on the 2D versions of the linear, quadratic, natural, and orthotropic smooth closures for reconstruction of the fourth-order orientation tensor. In contrast to the 3D case, a planar closure is defined by a single function of an eigenvalue of the second-order orientation tensor. In the absence of rotary diffusion, the natural closure is exact for isotropic initial conditions. A numerical study is performed for simple flows. The investigation of planar closures provides new insights and boundary conditions for the design of orthotropic closures in 3D. The proposed extensions use finite element shape functions to interpolate the data at principal orientation states and additional points. The results for 3D simple flows indicate that natural closures based on (extended) quadratic and piecewise-linear interpolation provide a far better description of the three-dimensional orientation dynamics than any other orthotropic closure considered in this study.

Keywords:
Fiber suspension flows, Jeffery's equation, Fokker-Planck equation, Fourier approximation, evolution of orientation tensors, orthotropic closures

Email address: kuzmin@math.uni-dortmund.de (Dmitri Kuzmin)

1. Introduction

The rheological behavior of fiber suspension flows is strongly influenced by the local orientation dynamics [11, 21]. Fiber-induced stresses are commonly modeled using orientation tensors which represent second- and fourth-order moments of the fiber orientation distribution. Evolution equations for these moments can be readily derived from the Fokker-Planck equation for the probability density function [1, 7]. However, the equation for an orientation tensor of order $2m$ requires a closure for the orientation tensor of order $2m + 2$. The need for such closures also arises in fiber orientation models based on spectral Galerkin methods for the Fokker-Planck equation [12, 13]. Whereas the second- and fourth-order orientation tensors are determined by the first coefficients of the spectral (Fourier in 2D, spherical harmonics in 3D) approximation to the probability density, the accuracy of numerical solutions depends on higher order coefficients which are expensive to calculate since a 3D transport equation must be solved for each space-dependent mode. The use of closure approximations to reconstruct the high-frequency components makes it possible to take the fine-scale effects into account at a fraction of the computational cost that a direct numerical simulation would require.

A variety of closure approximations for fiber suspensions and polymer flow models based on evolution equations for orientation tensors can be found in the literature. The simplest models assume a linear or quadratic relationship between the components of second- and fourth-order orientation tensors [1]. More realistic closures can be derived using a transformation to the principal axis coordinate system. In particular, this approach leads to a family of *orthotropic* closures [3, 4] in which unknown components of the transformed fourth-order tensor are approximated by linear or quadratic polynomials. Last but not least, analytical solutions of the Fokker-Planck equation can be used to derive *natural* closures which are exact if rotary diffusion is absent and the orientation distribution is isotropic at some point in time [6, 14, 15, 16, 19]. However, none of the existing closures can describe the rich variety of orientation states that may occur in real fiber suspension flows.

In this paper, we examine the planar versions of some basic closures in the principal axis representation and show that all of them reduce to simple functions of just one parameter which depends on an eigenvalue of the second-order orientation tensor. When it comes to the design of orthotropic closures

for three-dimensional models of orientation dynamics, we use planar closures to define the boundary conditions for polynomial fitting. In particular, this strategy leads to simple closed-form expressions for the orthotropic natural closure based on finite element interpolation. The numerical results compare favorably to those produced by other orthotropic closures.

2. Fiber orientation models

The orientation of a rigid rod-like fiber interacting with an incompressible velocity field $\mathbf{u}$ is described by a point $\mathbf{p} \in \mathbb{S}^d$ on the unit d-sphere

$$\mathbb{S}^d := \{\mathbf{p} \in \mathbb{R}^d \,:\, \|\mathbf{p}\| = 1\}, \quad d = 2, 3.$$

The orientation dynamics of single fibers and dilute fiber suspensions is governed by Jeffery's equation [9, 14]

$$\dot{\mathbf{p}} = \mathbf{W} \cdot \mathbf{p} + \lambda_e \left[\mathbf{D} \cdot \mathbf{p} - \mathbf{D} : (\mathbf{p} \otimes \mathbf{p}) \cdot \mathbf{p}\right], \tag{1}$$

where

$$\mathbf{D} = \frac{1}{2}\left[\nabla \mathbf{u} + (\nabla \mathbf{u})^T\right]$$

is the strain rate tensor,

$$\mathbf{W} = \frac{1}{2}\left[\nabla \mathbf{u} - (\nabla \mathbf{u})^T\right]$$

is the spin tensor and

$$\lambda_e = \frac{r_e^2 - 1}{r_e^2 + 1}$$

is a parameter which depends on the fiber aspect ratio $r_e := L/D$.

In Eulerian models of fiber suspension flows, the set of possible orientation states is described by an orientation distribution function ψ. The value of $\psi(\mathbf{x}, \mathbf{p}, t)$ corresponds to the probability that fibers located in a small neighborhood of point $\mathbf{x} \in \mathbb{R}^d$ have orientation $\mathbf{p} \in \mathbb{S}^d$ at time $t \geq 0$.

The evolution of ψ is governed by the Fokker-Planck equation [3, 7, 15]

$$\frac{\mathrm{d}\psi}{\mathrm{d}t} + \nabla_{\mathbf{p}} \cdot (\dot{\mathbf{p}}\psi) = D_r \Delta_{\mathbf{p}} \psi, \tag{2}$$

where $\frac{\mathrm{d}}{\mathrm{d}t} = \frac{\partial}{\partial t} + \mathbf{u}\cdot\nabla$ is the material time derivative, $\nabla_{\mathbf{p}}\cdot$ is the divergence operator defined on $\mathbb{S}^d$, and $\Delta_{\mathbf{p}}$ is the Laplace-Beltrami operator. The angular velocity $\dot{\mathbf{p}}$ of fiber rotation is defined by (1) and $D_r \geq 0$ is a rotary diffusion coefficient. It is commonly assumed that $D_r = 2C_I\dot{\gamma}$, where $\dot{\gamma} = \sqrt{\mathbf{D}:\mathbf{D}}$ and C_I is a constant that measures the intensity of fiber interactions [3, 7].

A simplified description of the local orientation state is provided by moments of ψ. The orientation tensors of second and fourth order are defined by

$$\mathbf{A} = \int_{\mathbb{S}^d} \mathbf{p}\otimes\mathbf{p}\ \psi(\mathbf{p})\,\mathrm{d}\mathbf{p} = \{A_{ij}\}_{i,j=1}^{d}\,, \tag{3}$$

$$\mathbb{A} = \int_{\mathbb{S}^d} \mathbf{p}\otimes\mathbf{p}\otimes\mathbf{p}\otimes\mathbf{p}\ \psi(\mathbf{p})\,\mathrm{d}\mathbf{p} = \{A_{ijkl}\}_{i,j,k,l=1}^{d}\,. \tag{4}$$

An evolution equation for $\mathbf{A}$ can be readily derived by taking the second moment of the Fokker-Planck equation (2) which can be written as [1, 7]

$$\frac{\mathrm{d}\mathbf{A}}{\mathrm{d}t} = \mathbf{W}\cdot\mathbf{A} - \mathbf{A}\cdot\mathbf{W} + \lambda_e\left[\mathbf{A}\cdot\mathbf{D} + \mathbf{D}\cdot\mathbf{A} - 2\mathbb{A}:\mathbf{D}\right] + 2D_r(\mathbf{I} - d\mathbf{A}). \tag{5}$$

Since the right-hand side of this equation depends on the fourth-order orientation tensor $\mathbb{A}$, a suitable *closure* must be provided to reconstruct $\mathbb{A}$ and/or the probability distribution ψ from the second-order moment $\mathbf{A}$.

In the case $D_r = 0$, the analytical solution of the initial value problem

$$\frac{\mathrm{d}\psi}{\mathrm{d}t} + \nabla_{\mathbf{p}}\cdot(\dot{\mathbf{p}}\psi) = 0, \qquad \psi|_{t=0} = \psi_0 \tag{6}$$

is given by [14]

$$\psi(\mathbf{p}) = \psi_0\left(\frac{\mathbf{C}\mathbf{p}}{\|\mathbf{C}\mathbf{p}\|}\right)\frac{1}{\|\mathbf{C}\mathbf{p}\|^d}, \quad d = 2, 3, \tag{7}$$

$$\frac{\mathrm{d}\mathbf{C}}{\mathrm{d}t} = -\mathbf{C}\cdot(\mathbf{W} + \lambda_e\mathbf{D}), \quad \mathbf{C}|_{t=0} = \mathbf{I}, \tag{8}$$

where $\mathbf{I}$ is the identity tensor. Hence, the exact solution to the Fokker-Planck equation can be determined by evolving the second-order tensor $\mathbf{C}$.

In the case of the isotropic initial distribution, we have

$$\psi_0(\mathbf{p}) = \frac{1}{2(d-1)\pi}, \quad d = 2, 3 \tag{9}$$

and, therefore,

$$\psi(\mathbf{p}) = \frac{1}{2(d-1)\pi} \frac{1}{\|\mathbf{C}\mathbf{p}\|^d} = \frac{1}{2(d-1)\pi} \frac{1}{(\mathbf{B} : (\mathbf{p} \otimes \mathbf{p}))^{d/2}}, \tag{10}$$

where $\mathbf{B} = \mathbf{C}^T\mathbf{C}$. Substituting (10) into (3), one obtains

$$\mathbf{A} = \frac{1}{2(d-1)\pi} \int_{\mathbb{S}^d} \frac{\mathbf{p} \otimes \mathbf{p}}{(\mathbf{B} : (\mathbf{p} \otimes \mathbf{p}))^{d/2}} \, \mathrm{d}\mathbf{p}. \tag{11}$$

By definition, $\mathbf{A}$ and $\mathbf{B}$ are symmetric positive-definite tensors satisfying

$$\mathrm{tr}\mathbf{A} = \sum_{i=1}^{d} \lambda_i = 1$$

and

$$\det \mathbf{B} = \prod_{i=1}^{d} \mu_i = 1,$$

where $\lambda_i \geq 0$ and $\mu_i > 0$ are the real principal values of the two tensors.

Importantly, $\mathbf{A}$ and $\mathbf{B}$ are simultaneously diagonalizable. If $\mathbf{B} = \mathbf{Q}\hat{\mathbf{B}}\mathbf{Q}^T$, where $\hat{\mathbf{B}}$ is a diagonal tensor and $\mathbf{Q}$ is an orthogonal transformation, then

$$\begin{aligned} \mathbf{A} &= \frac{1}{2(d-1)\pi} \int_{\mathbb{S}^d} \frac{\mathbf{p} \otimes \mathbf{p}}{(\mathbf{p} \cdot \mathbf{Q}\hat{\mathbf{B}}\mathbf{Q}^T\mathbf{p})^{d/2}} \, \mathrm{d}\mathbf{p} \\ &= \frac{1}{2(d-1)\pi} \int_{\mathbb{S}^d} \frac{\mathbf{Q}\hat{\mathbf{p}} \otimes \hat{\mathbf{p}}\mathbf{Q}^T}{(\hat{\mathbf{p}} \cdot \hat{\mathbf{B}}\hat{\mathbf{p}})^{d/2}} \, \mathrm{d}\hat{\mathbf{p}} = \mathbf{Q}\hat{\mathbf{A}}\mathbf{Q}^T, \end{aligned}$$

where $\hat{\mathbf{p}} = \mathbf{Q}^T\mathbf{p}$ is the orientation in the initial reference frame and

$$\hat{\mathbf{A}} = \frac{1}{2(d-1)\pi} \int_{\mathbb{S}^d} \frac{\hat{\mathbf{p}} \otimes \hat{\mathbf{p}}}{(\hat{\mathbf{p}} \cdot \hat{\mathbf{B}}\hat{\mathbf{p}})^{d/2}} \, \mathrm{d}\hat{\mathbf{p}}$$

is diagonal since $\mathbf{A}(0) = \hat{\mathbf{A}}(0)$ is diagonal for random initial distributions.

As shown by Montgomery-Smith et al. [14], the (nonlinear) relationship (11) between $\mathbf{A}$ and $\mathbf{B}$ is one-to-one and can be used to reconstruct

$$\mathbb{A} = \frac{1}{2(d-1)\pi} \int_{\mathbb{S}^d} \frac{\mathbf{p} \otimes \mathbf{p} \otimes \mathbf{p} \otimes \mathbf{p}}{(\mathbf{B} : (\mathbf{p} \otimes \mathbf{p}))^{d/2}} \, \mathrm{d}\mathbf{p}. \tag{12}$$

This closure is exact for orientation distributions that are isotropic at some point in evolution history. Instead of calculating $\mathbf{B}$ from $\mathbf{A}$ using formula (11), one can evolve $\mathbf{B}$ using the differential equation [14]

$$\frac{\mathrm{d}\mathbf{B}}{\mathrm{d}t} = \mathbf{W}\cdot\mathbf{B} - \mathbf{B}\cdot\mathbf{W} - \lambda_e(\mathbf{B}\cdot\mathbf{D} + \mathbf{D}\cdot\mathbf{B}) = 0, \quad \mathbf{B}|_{t=0} = \mathbf{I}. \tag{13}$$

Efforts aimed at extending this approach to Brownian fiber suspensions ($D_r > 0$) have led to the development of the deformation tensor model [18] and of the *fast exact closure* for Jeffery's equation with diffusion [15].

Closures based on solving a differential equation for $\mathbf{B}$ may offer considerable savings as long as the time derivative does not incorporate a spatial advection operator. Otherwise, the cost of evolving $\mathbf{B}$ becomes rather high and no exact solvers are available for the space-dependent transport equation. For this reason, we favor simple reconstruction-based closures in this work.

3. Two-dimensional orientation dynamics

The presentation of closure approximations in the literature on fiber suspension flow modeling [3, 14, 15] is usually focused on the general three-dimensional setting ($d = 3$). A notable extension to this rule is the work of Altan and Tang [2] in which planar orientation patterns are studied for simple flows of dilute suspensions. Planar versions of some popular closure approximations are also considered in [16]. Whereas 2D models of fiber orientation are of limited practical utility *per se*, it is instructive to begin with a closer investigation of planar closures. As we will see, this bottom-up approach reveals interesting relationships between existing closures and provides additional information for derivation of new three-dimensional extensions.

3.1. Planar orientation tensors

In the two-dimensional case, the polar coordinate representation of $\mathbf{p} \in \mathbb{S}^2$ is

$$\mathbf{p} = \begin{bmatrix} p_1 \\ p_2 \end{bmatrix} = \begin{bmatrix} \cos\varphi \\ \sin\varphi \end{bmatrix}, \qquad \varphi \in [0, 2\pi).$$

As shown by Lohmann [12, 13], moments of a planar orientation distribution

$$\psi : \mathbb{S}^2 \to \mathbb{R}_+, \qquad \psi(\mathbf{p}) = \psi(-\mathbf{p})$$

are associated with the coefficients of the Fourier series

$$\psi(\mathbf{p}(\varphi)) = a_0 + \sum_{k=1}^{\infty}(a_k \cos(k\varphi) + b_k \sin(k\varphi)) =: \tilde{\psi}(\varphi), \tag{14}$$

where

$$a_0 = \frac{1}{2\pi}\int_0^{2\pi} \tilde{\psi}(\varphi)d\varphi, \tag{15}$$

$$a_k = \frac{1}{\pi}\int_0^{2\pi} \cos(k\varphi)\tilde{\psi}(\varphi)d\varphi, \quad k \in \mathbb{N}, \tag{16}$$

$$b_k = \frac{1}{\pi}\int_0^{2\pi} \sin(k\varphi)\tilde{\psi}(\varphi)d\varphi, \quad k \in \mathbb{N}. \tag{17}$$

Since $\tilde{\psi}$ is a probability density satisfying the normalization condition

$$\int_0^{2\pi} \tilde{\psi}(\varphi)d\varphi = 1,$$

we have

$$a_0 = \frac{1}{2\pi}. \tag{18}$$

By definition (3), the coefficients of the orientation tensor $\mathbf{A}$ are given by

$$A_{ij} = \int_0^{2\pi} p_i(\varphi)p_j(\varphi)\tilde{\psi}(\varphi)\mathrm{d}\varphi, \quad i,j = 1,2, \tag{19}$$

$$p_1(\varphi) = \cos\varphi, \quad p_2(\varphi) = \sin\varphi.$$

This yields

$$\mathbf{A} = \frac{\pi}{2}\begin{bmatrix} 2a_0 + a_2 & b_2 \\ b_2 & 2a_0 - a_2 \end{bmatrix} := \begin{bmatrix} \alpha_1 & \alpha_2 \\ \alpha_2 & \alpha_3 \end{bmatrix}. \tag{20}$$

The relationship between $\alpha_1, \alpha_2, \alpha_3$ and the first coefficients of the Fourier series (14) is given by the linear transformation

$$\begin{bmatrix} \alpha_1 \\ \alpha_2 \\ \alpha_3 \end{bmatrix} = \frac{\pi}{2}\begin{bmatrix} 2 & 1 & 0 \\ 0 & 0 & 1 \\ 2 & -1 & 0 \end{bmatrix}\begin{bmatrix} a_0 \\ a_2 \\ b_2 \end{bmatrix}. \tag{21}$$

Invoking (18) we find that $\mathbf{A}$ must satisfy the unit trace condition

$$A_{11} + A_{22} = \alpha_1 + \alpha_3 = 2\pi a_0 = 1 \tag{22}$$

which implies that

$$\alpha_3 = 1 - \alpha_1. \tag{23}$$

A general fourth-order tensor $\mathbb{A}$ can be written in the 4×4 matrix form

$$\underline{\mathbb{A}} := \begin{bmatrix} A_{1111} & A_{1121} & A_{1112} & A_{1122} \\ A_{2111} & A_{2121} & A_{2112} & A_{2122} \\ A_{1211} & A_{1221} & A_{1212} & A_{1222} \\ A_{2211} & A_{2221} & A_{2212} & A_{2222} \end{bmatrix} \in \mathbb{R}^{4\times 4}. \tag{24}$$

By definition (3), the coefficients of the orientation tensor $\mathbb{A}$ are given by

$$A_{ijkl} = \int_0^{2\pi} p_i(\varphi)p_j(\varphi)p_k(\varphi)p_l(\varphi)\tilde{\psi}(\varphi)\mathrm{d}\varphi = \underline{\mathbb{A}}_{IJ}, \qquad i,j,k,l = 1,2, \tag{25}$$

$$I = i + 2(j-1), \quad J = k + 2(l-1), \qquad I, J \in \{1, \ldots, 4\}.$$

The entries of the corresponding 4×4 matrix

$$\begin{aligned} \underline{\mathbb{A}} = \frac{\pi}{8} \begin{bmatrix} 6a_0 + 4a_2 + a_4 & 2b_2 + b_4 & 2b_2 + b_4 & 2a_0 - a_4 \\ 2b_2 + b_4 & 2a_0 - a_4 & 2a_0 - a_4 & 2b_2 - b_4 \\ 2b_2 + b_4 & 2a_0 - a_4 & 2a_0 - a_4 & 2b_2 - b_4 \\ 2a_0 - a_4 & 2b_2 - b_4 & 2b_2 - b_4 & 6a_0 - 4a_2 + a_4 \end{bmatrix} \\ =: \begin{bmatrix} \gamma_1 & \gamma_2 & \gamma_2 & \gamma_3 \\ \gamma_2 & \gamma_3 & \gamma_3 & \gamma_4 \\ \gamma_2 & \gamma_3 & \gamma_3 & \gamma_4 \\ \gamma_3 & \gamma_4 & \gamma_4 & \gamma_5 \end{bmatrix} \end{aligned} \tag{26}$$

are related to the first Fourier coefficients by the linear mapping

$$\begin{bmatrix} \gamma_1 \\ \gamma_2 \\ \gamma_3 \\ \gamma_4 \\ \gamma_5 \end{bmatrix} = \frac{\pi}{8} \begin{bmatrix} 6 & 4 & 1 & 0 & 0 \\ 0 & 0 & 0 & 2 & 1 \\ 2 & 0 & -1 & 0 & 0 \\ 0 & 0 & 0 & 2 & -1 \\ 6 & -4 & 1 & 0 & 0 \end{bmatrix} \begin{bmatrix} a_0 \\ a_2 \\ a_4 \\ b_2 \\ b_4 \end{bmatrix}. \tag{27}$$

By (20), (24) and (26), a well-designed closure must satisfy

$$\gamma_1 + \gamma_3 = A_{11}, \quad \gamma_2 + \gamma_4 = A_{12}, \quad \gamma_3 + \gamma_5 = A_{22} \tag{28}$$

and the following set of symmetry conditions:

$$A_{1121} = A_{1112} = A_{2111} = A_{1211} = \gamma_2, \tag{29}$$

$$A_{1122} = A_{2121} = A_{2112} = A_{1221} = A_{1212} = A_{2211} = \gamma_3, \tag{30}$$

$$A_{2221} = A_{2212} = A_{2122} = A_{1222} = \gamma_4. \tag{31}$$

Due to symmetry, the entries of $\underline{\mathbb{A}}$ could be stored in a 3×3 matrix obtained from (26) by deleting the second row and column. In this section, we will exploit existing symmetries but use the general 4×4 matrix form of $\mathbb{A}$.

3.2. Basic planar closures

The following closures can be used to reconstruct the fourth-order tensor $\mathbb{A}$ from its second-order counterpart $\mathbf{A}$ or, equivalently, the Fourier coefficients a_4, b_4 from a_0, a_2, b_2 in planar models of orientation dynamics [16]:

- Linear closure

$$\begin{aligned} A_{ijkl} = \frac{1}{6}(&A_{ij}\delta_{kl} + A_{ik}\delta_{jl} + A_{il}\delta_{jk} + A_{kl}\delta_{ij} + A_{jl}\delta_{ik} + A_{jk}\delta_{il}) \\ &- \frac{1}{24}(\delta_{ij}\delta_{kl} + \delta_{ik}\delta_{jl} + \delta_{il}\delta_{jk}). \end{aligned} \tag{32}$$

- Quadratic closure

$$A_{ijkl} = A_{ij}A_{kl}. \tag{33}$$

- Natural closure [6, 19]

$$\begin{aligned} A_{ijkl} = &\frac{1}{6}\det(\mathbf{A})(\delta_{ij}\delta_{kl} + \delta_{ik}\delta_{jl} + \delta_{il}\delta_{jk}) \\ &+ \frac{1}{3}(A_{ij}A_{kl} + A_{ik}A_{jl} + A_{il}A_{jk}). \end{aligned} \tag{34}$$

By (18), (24) and (26), the linear closure is equivalent to truncation:

$$\begin{aligned} a_4 &= 2a_0 - \frac{8}{\pi}A_{1122} = 2a_0 - \frac{8}{\pi}\left(\frac{A_{11} + A_{22}}{6} - \frac{1}{24}\right) = \frac{1}{\pi} - \frac{1}{\pi} = 0, \\ b_4 &= \frac{4}{\pi}(A_{2111} - A_{2122}) = \frac{4}{\pi}\left(\frac{1}{2}A_{21} - \frac{1}{2}A_{21}\right) = 0. \end{aligned}$$

The quadratic closure (33) satisfies compatibility conditions (29) and (31), whereas condition (30) reduces to $A_{11}A_{22} = A_{12}^2$. Thus the real eigenvalues λ_1 and λ_2 of the symmetric second-order tensor $\mathbf{A}$ must satisfy

$$\lambda_1\lambda_2 = \det \mathbf{A} = A_{11}A_{22} - A_{12}^2 = 0,$$

$$\lambda_1 + \lambda_2 = \mathrm{tr}\mathbf{A} = A_{11} + A_{22} = 1.$$

It follows that condition (30) is satisfied for fully aligned orientation states ($\lambda_1 = 1,\ \lambda_2 = 0$ or $\lambda_1 = 0,\ \lambda_2 = 1$) but the structure of (26) is not preserved in general. As a consequence, the one-to-one relationship between the entries of $\underline{\mathbb{A}}$ and the Fourier coefficients of ψ is lost. To remedy this inconsistency, we consider a modified quadratic closure defined by (26) with

$$\gamma_1 = A_{11}A_{11}, \quad \gamma_2 = A_{11}A_{12}, \quad \gamma_3 = A_{11}A_{22},$$

$$\gamma_4 = A_{22}A_{12}, \quad \gamma_5 = A_{22}A_{22}.$$

The above values of $\gamma_2, \gamma_3, \gamma_4$ are chosen because they satisfy both the closure relation (33) and conditions (28). Indeed, we have

$$\begin{aligned}
\gamma_1 + \gamma_3 &= A_{11}(A_{11} + A_{22}) = A_{11},\\
\gamma_2 + \gamma_4 &= (A_{11} + A_{22})A_{12} = A_{12},\\
\gamma_3 + \gamma_5 &= A_{22}(A_{11} + A_{22}) = A_{22}.
\end{aligned}$$

The natural closure (34) of Verleye and Dupret [6, 19] is equivalent to the exact closure (12) for $D_r = 0$. We verify this in Appendix A for $d = 2$.

3.3. Transformation of coordinates

The number of degrees of freedom to be modeled can be reduced using a transformation to the principal axes of the second-order tensor $\mathbf{A}$. A detailed description of transformation procedures for the general 3D case can be found, e.g., in [17]. In the present paper, we derive planar counterparts of orthotropic closures [3] in the principal axis system using the following rules to transform the second- and fourth-order orientation tensors in 2D.

The second-order tensor $\mathbf{A}$ is symmetric and positive semi-definite. Therefore, it possesses two real nonnegative eigenvalues

$$\lambda_1 =: \lambda, \quad \lambda_2 = 1 - \lambda, \quad \lambda \in [0, 1] \tag{35}$$

and a set of two orthogonal eigenvectors $\{\mathbf{q}_1, \mathbf{q}_2\}$ such that

$$\hat{\mathbf{A}} = \begin{bmatrix} \lambda & 0 \\ 0 & 1-\lambda \end{bmatrix} = \mathbf{Q}\mathbf{A}\mathbf{Q}^T, \qquad \mathbf{Q}^T = [\mathbf{q}_1, \mathbf{q}_2]. \tag{36}$$

Introducing the vector notation for general second-order tensors

$$\underline{\mathbf{A}} = [A_{11}, A_{21}, A_{12}, A_{22}]^T, \tag{37}$$

the linear transformation defined by (36) can be written as

$$\underline{\hat{\mathbf{A}}} = \underline{\mathbb{Q}}\, \underline{\mathbf{A}}, \tag{38}$$

where $\underline{\mathbb{Q}} \in \mathbb{R}^{4\times 4}$ is the matrix form of a fourth-order tensor $\mathbb{Q}$.

Using the representation of $\mathbf{A}$ as a linear combination of dyadic products

$$\mathbf{A} = \sum_{i=1}^{2}\sum_{j=1}^{2} A_{ij}\mathbf{E}_{ij}, \qquad \mathbf{E}_{ij} = \mathbf{e}_i \otimes \mathbf{e}_j,$$

we find that

$$\hat{\mathbf{A}} = \sum_{i=1}^{2}\sum_{j=1}^{2} A_{ij}\hat{\mathbf{E}}_{ij}, \qquad \hat{\mathbf{E}}_{ij} = \mathbf{Q}\mathbf{E}_{ij}\mathbf{Q}^T.$$

In matrix notation, this dyadic product decomposition corresponds to

$$\underline{\hat{\mathbf{A}}} = \sum_{i=1}^{4} A_i \underline{\hat{\mathbf{E}}}_i, \qquad \underline{\hat{\mathbf{E}}}_i = \underline{\mathbb{Q}}\ \underline{\mathbf{E}}_i,$$

where $\underline{\mathbf{E}}_i$ is the unit vector form of a dyadic product tensor

$$\underline{\mathbf{E}}_i = [\delta_{i1}, \delta_{i2}, \delta_{i3}, \delta_{i4}]^T$$

and $\underline{\hat{\mathbf{E}}}_i$ is the i-th column of the transformation matrix $\underline{\mathbb{Q}}$. We have

$$\hat{\mathbf{E}}_{11} = \begin{bmatrix} Q_{11} & Q_{12} \\ Q_{21} & Q_{22} \end{bmatrix} \begin{bmatrix} 1 & 0 \\ 0 & 0 \end{bmatrix} \begin{bmatrix} Q_{11} & Q_{21} \\ Q_{12} & Q_{22} \end{bmatrix} = \begin{bmatrix} Q_{11}Q_{11} & Q_{11}Q_{21} \\ Q_{11}Q_{21} & Q_{21}Q_{21} \end{bmatrix},$$

$$\hat{\mathbf{E}}_{21} = \begin{bmatrix} Q_{11} & Q_{12} \\ Q_{21} & Q_{22} \end{bmatrix} \begin{bmatrix} 0 & 0 \\ 1 & 0 \end{bmatrix} \begin{bmatrix} Q_{11} & Q_{21} \\ Q_{12} & Q_{22} \end{bmatrix} = \begin{bmatrix} Q_{11}Q_{12} & Q_{21}Q_{12} \\ Q_{11}Q_{22} & Q_{21}Q_{22} \end{bmatrix},$$

$$\hat{\mathbf{E}}_{12} = \begin{bmatrix} Q_{11} & Q_{12} \\ Q_{21} & Q_{22} \end{bmatrix} \begin{bmatrix} 0 & 1 \\ 0 & 0 \end{bmatrix} \begin{bmatrix} Q_{11} & Q_{21} \\ Q_{12} & Q_{22} \end{bmatrix} = \begin{bmatrix} Q_{11}Q_{12} & Q_{11}Q_{22} \\ Q_{21}Q_{12} & Q_{21}Q_{22} \end{bmatrix},$$
$$\hat{\mathbf{E}}_{22} = \begin{bmatrix} Q_{11} & Q_{12} \\ Q_{21} & Q_{22} \end{bmatrix} \begin{bmatrix} 0 & 0 \\ 0 & 1 \end{bmatrix} \begin{bmatrix} Q_{11} & Q_{21} \\ Q_{12} & Q_{22} \end{bmatrix} = \begin{bmatrix} Q_{12}Q_{12} & Q_{12}Q_{22} \\ Q_{12}Q_{22} & Q_{22}Q_{22} \end{bmatrix}.$$

Thus the matrix $\underline{\mathbb{Q}}$ of the orthogonal transformation is given by

$$\underline{\mathbb{Q}} = \begin{bmatrix} Q_{11}Q_{11} & Q_{11}Q_{12} & Q_{11}Q_{12} & Q_{12}Q_{12} \\ Q_{11}Q_{21} & Q_{11}Q_{22} & Q_{21}Q_{12} & Q_{12}Q_{22} \\ Q_{11}Q_{21} & Q_{21}Q_{12} & Q_{11}Q_{22} & Q_{12}Q_{22} \\ Q_{21}Q_{21} & Q_{21}Q_{22} & Q_{21}Q_{22} & Q_{22}Q_{22} \end{bmatrix}. \tag{39}$$

Applying this matrix to the vector form $\underline{\mathbf{S}} = \underline{\mathbb{A}}\,\underline{\mathbf{D}}$ of the second-order tensor $\mathbf{S} = \mathbb{A} : \mathbf{D}$ which requires a closure approximation, we obtain

$$\hat{\underline{\mathbf{S}}} = \mathbb{Q}\underline{\mathbf{S}} = \mathbb{Q}\underline{\mathbb{A}}\,\underline{\mathbf{D}} = \mathbb{Q}\underline{\mathbb{A}}\underline{\mathbb{Q}}^T\underline{\mathbb{Q}}\,\underline{\mathbf{D}} = \mathbb{Q}\underline{\mathbb{A}}\underline{\mathbb{Q}}^T\hat{\underline{\mathbf{D}}} = \hat{\underline{\mathbb{A}}}\,\hat{\underline{\mathbf{D}}},$$

where

$$\hat{\underline{\mathbb{A}}} = \mathbb{Q}\underline{\mathbb{A}}\underline{\mathbb{Q}}^T. \tag{40}$$

An orientation state $\hat{\underline{\mathbb{A}}}$ is invariant under an orthogonal transformation defined by the matrix $\underline{\mathbb{P}}$ of the linear mapping if and only if

$$\hat{\underline{\mathbb{A}}} = \underline{\mathbb{P}}\,\hat{\underline{\mathbb{A}}}\,\underline{\mathbb{P}}^T. \tag{41}$$

The pure reflection corresponds to

$$\underline{\mathbb{P}} = \begin{bmatrix} 1 & 0 & 0 & 0 \\ 0 & -1 & 0 & 0 \\ 0 & 0 & -1 & 0 \\ 0 & 0 & 0 & 1 \end{bmatrix}.$$

By (41), the so-defined transformation is invariant if the matrices

$$\hat{\underline{\mathbb{A}}} = \begin{bmatrix} \hat{\gamma}_1 & \hat{\gamma}_2 & \hat{\gamma}_2 & \hat{\gamma}_3 \\ \hat{\gamma}_2 & \hat{\gamma}_3 & \hat{\gamma}_3 & \hat{\gamma}_4 \\ \hat{\gamma}_2 & \hat{\gamma}_3 & \hat{\gamma}_3 & \hat{\gamma}_4 \\ \hat{\gamma}_3 & \hat{\gamma}_4 & \hat{\gamma}_4 & \hat{\gamma}_5 \end{bmatrix}$$

and

$$\underline{\mathbb{P}}\,\underline{\hat{\mathbb{A}}}\,\underline{\mathbb{P}}^T = \begin{bmatrix} \hat{\gamma}_1 & -\hat{\gamma}_2 & -\hat{\gamma}_2 & \hat{\gamma}_3 \\ -\hat{\gamma}_2 & \hat{\gamma}_3 & \hat{\gamma}_3 & -\hat{\gamma}_4 \\ -\hat{\gamma}_2 & \hat{\gamma}_3 & \hat{\gamma}_3 & -\hat{\gamma}_4 \\ \hat{\gamma}_3 & -\hat{\gamma}_4 & -\hat{\gamma}_4 & \hat{\gamma}_5 \end{bmatrix}$$

are equal. Thus, an invariant closure approximation must satisfy

$$\hat{\gamma}_2 = \hat{\gamma}_4 = 0$$

and produce

$$\underline{\hat{\mathbb{A}}} = \begin{bmatrix} \hat{\gamma}_1 & 0 & 0 & \hat{\gamma}_3 \\ 0 & \hat{\gamma}_3 & \hat{\gamma}_3 & 0 \\ 0 & \hat{\gamma}_3 & \hat{\gamma}_3 & 0 \\ \hat{\gamma}_3 & 0 & 0 & \hat{\gamma}_5 \end{bmatrix}. \tag{42}$$

By virtue of (28), two degrees of freedom are defined by the constraints

$$\begin{aligned} \hat{\gamma}_1 + \hat{\gamma}_3 &= \lambda_1 = \lambda, \\ \hat{\gamma}_1 + \hat{\gamma}_5 &= \lambda_2 = 1 - \lambda. \end{aligned}$$

To define a general closure, it is sufficient to provide an approximation to

$$\hat{\gamma}_3(\lambda) = f(\lambda). \tag{43}$$

The values of the remaining two parameters are defined by

$$\hat{\gamma}_1(\lambda) = \lambda - \hat{\gamma}_3(\lambda), \tag{44}$$

$$\hat{\gamma}_5(\lambda) = 1 - \lambda - \hat{\gamma}_3(\lambda). \tag{45}$$

The inverse orthogonal transformation yields the matrix

$$\underline{\mathbb{A}} = \underline{\mathbb{Q}}^T \underline{\hat{\mathbb{A}}}\,\underline{\mathbb{Q}} \tag{46}$$

containing the coefficients of the fourth-order orientation tensor.

3.4. Unified planar closures

Using the above transformation to the principal axes, planar closure approximations can be designed by fitting the coefficients of a polynomial

$$\hat{\gamma}_3(\lambda) = c_0 + c_1\lambda + c_2\lambda^2 + \dots \tag{47}$$

to a set of discrete values or derivatives of $\hat{\gamma}_3$ at certain points. In the *orthotropic smooth* closure of Cintra and Tucker [3], linear interpolation is used between smooth orientation states associated with aligned and isotropic probability distributions. In *orthotropic fitted* closures [3, 4], least-squares fitting is performed using numerical solutions to the Fokker-Planck equation for simple flows. The data set for polynomial fitting can also be generated using the analytical solution (7) for $D_r = 0$ [14, 20]. Similar approaches can be used to construct polynomial closure approximations in the planar case. The representation of the fourth-order orientation tensor in the principal axis form reveals some interesting relationships between the basic closures presented in Section 3.2 and provides a convenient unified framework for the design of new closures based on polynomial fitting techniques.

Without loss of generality, we define $\hat{\gamma}_3(\lambda)$ for $\lambda \in [0, \frac{1}{2}]$ in the planar case. Figure 1 displays the graphs of the following closure approximations:

- Linear closure
$$\hat{\gamma}_3(\lambda) \equiv \frac{1}{8}. \tag{48}$$
- Smooth closure
$$\hat{\gamma}_3(\lambda) = \frac{1}{2}\lambda. \tag{49}$$
- Quadratic closure
$$\hat{\gamma}_3(\lambda) = \lambda(1-\lambda). \tag{50}$$
- Natural closure
$$\hat{\gamma}_3(\lambda) = \frac{1}{2}\lambda(1-\lambda). \tag{51}$$
- Mixed closure
$$\hat{\gamma}_3(\lambda) = \min\left\{\frac{1}{8}, \frac{1}{2}\lambda\right\}. \tag{52}$$

The new mixed closure represents a piecewise-linear fit to (48),(49), and (51).

Interestingly enough, the principal axis forms of the quadratic and natural closures differ only by a constant factor of $\frac{1}{2}$. The new mixed closure (52)

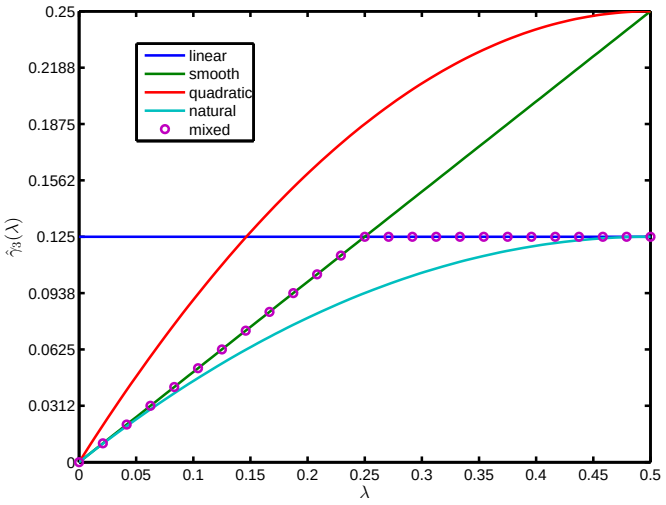

Figure 1: Planar closures in the principal axis system.

represents a piecewise-linear counterpart of the natural closure (51). Note that both (51) and (52) satisfy the boundary conditions

$$\hat{\gamma}_3(0) = 0, \quad \hat{\gamma}_3'(0) = \frac{1}{2}, \quad \hat{\gamma}_3\left(\frac{1}{2}\right) = \frac{1}{8}, \quad \hat{\gamma}_3'\left(\frac{1}{2}\right) = 0$$

which are exact in the case $D_r = 0$. The linear closure produces $\hat{\gamma}_3(0) = \frac{1}{8}$ and $\hat{\gamma}_3'(0) = 0$ for aligned orientation states. The smooth and quadratic closures satisfy $\hat{\gamma}_3\left(\frac{1}{2}\right) = \frac{1}{4}$ for isotropic probability distributions. In contrast to all other closures, the slope $\hat{\gamma}_3'\left(\frac{1}{2}\right)$ of the smooth closure equals $\frac{1}{2}$. A numerical study of approximations (48)–(52) is presented in Section 3.5.

3.5. Numerical study of planar closures

In this section, we perform a numerical study of the above planar closures for simple 2D flows. Equation (5) with $\lambda_e = \frac{99}{101}$, $D_r = 0$ is solved numerically using the explicit Euler method and the time step $\Delta t = 0.1$. The Frobenius norm is used to measure the error in the components of the second-order orientation tensor $\mathbf{A}$ for $0 \le t \le T = 150$. The reference solution $\mathbf{A}_{\text{ex}}$ is calculated using definition (3) and the probability density distribution ψ given by (7). The differential equation (8) for the second-order deformation tensor $\mathbf{C}$ is solved analytically using the formulas presented in [2, 12].

Figure 2 shows the evolution of errors in numerical solutions produced by the five closure approximations for the following velocity gradients:

- Flow 1: *Planar elongation*

$$\nabla \mathbf{u} = \begin{bmatrix} 0.01 & 0.0 \\ 0.0 & -0.01 \end{bmatrix}.$$

- Flow 2: *Simple shear*

$$\nabla \mathbf{u} = \begin{bmatrix} 0.0 & 0.01 \\ 0.0 & 0.0 \end{bmatrix}.$$

- Flow 3: *Shearing and stretching*

$$\nabla \mathbf{u} = \begin{bmatrix} 0.01 & 0.01 \\ -0.01 & -0.01 \end{bmatrix}.$$

For each flow pattern, two different sets of Fourier coefficients are used to define the initial orientation state $\mathbf{A}(0)$ using (20). The initial condition

$$a_0 = \frac{1}{2\pi}, \quad a_2 = 0, \quad b_2 = 0$$

corresponds to the isotropic orientation distribution. The results presented in the left diagrams of Fig. 2 confirm that the natural closure is exact for this particular choice of initial conditions. The results presented in the right diagrams were obtained using $\mathbf{A}(0)$ defined by the Fourier coefficients

$$a_0 = \frac{1}{2\pi}, \quad a_2 = 0.1, \quad b_2 = 0.$$

Remarkably, the piecewise-linear mixed closure performs better than the natural closure when this initial condition is used for Flow 1 in Fig. 2(b).

In all diagrams, the error curve of the mixed closure follows the linear closure curve as long as the error is smaller than that of the smooth closure. Then the two curves separate and the error of the mixed closure begins to decrease whereas the error of the linear closure increases monotonically. The error plots for Flow 2 resemble a zoom of the corresponding diagrams for Flows 1

and 3. This indicates that the orientation dynamics changes in the same way but on different time scales for the simple flows under consideration.

The error curves of the smooth and quadratic closures coincide in Fig. 2(b), and there is hardly any difference between the curves of the linear and mixed closures in Fig. 2(b) because they begin to separate at the end of the time interval $[0, 150]$. In summary, the best results are produced by the natural and mixed closures followed by the smooth and quadratic closures. The linear closure performs well as long as the orientation distribution remains close to the isotropic state ($\lambda = \frac{1}{2}$) but becomes very inaccurate as the difference between the eigenvalues of the second-order orientation tensor increases.

4. Three-dimensional orientation dynamics

Let us now consider the general three-dimensional case in which $\mathbb{S}^3$ is the unit sphere in $\mathbb{R}^3$ and the spherical coordinate representation

$$\mathbf{p} = \begin{bmatrix} p_1 \\ p_2 \\ p_3 \end{bmatrix} = \begin{bmatrix} \sin\theta\cos\varphi \\ \sin\theta\sin\varphi \\ \cos\theta \end{bmatrix}, \qquad \varphi \in [0, 2\pi), \quad \theta \in [0, \pi]$$

of the orientation vector $\mathbf{p} \in \mathbb{S}^3$ is adopted. The orientation distribution

$$\tilde{\psi}(\theta, \varphi) := \psi(\mathbf{p}(\theta, \varphi))$$

becomes a function of two angles and its moments are defined by

$$A_{ij} = \int_0^{2\pi} \int_0^{\pi} p_i(\theta, \varphi) p_j(\theta, \varphi) \tilde{\psi}(\theta, \varphi) \sin\theta \mathrm{d}\theta \mathrm{d}\varphi, \quad i, j = 1, 2, 3 \tag{53}$$

$$A_{ijkl} = \int_0^{2\pi} \int_0^{\pi} p_i(\theta, \varphi) p_j(\theta, \varphi) p_k(\theta, \varphi) p_l(\theta, \varphi) \tilde{\psi}(\theta, \varphi) \sin\theta \mathrm{d}\theta \mathrm{d}\varphi, \tag{54}$$
$$i, j, k, l = 1, 2, 3.$$

By this definition, the fourth-order orientation tensor $\mathbb{A}$ is symmetric with respect to any pair of indices. That is, we have [3]

$$A_{ijkl} = A_{jikl} = A_{ijlk} = A_{kjil} = A_{ljki} = A_{ikjl} = A_{ilkj}. \tag{55}$$

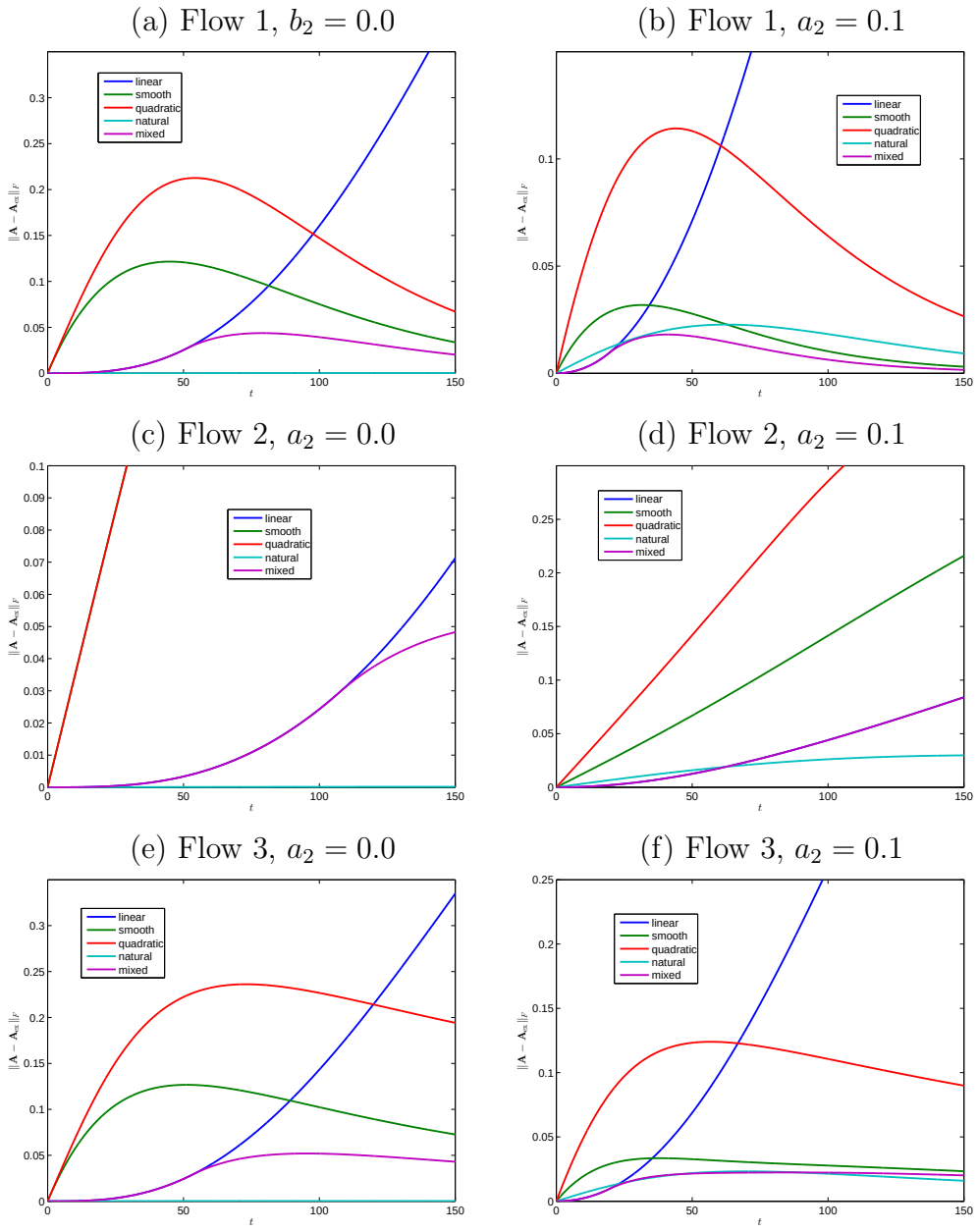

Figure 2: Numerical study of unified planar closures for simple flows: Frobenius norm of the error in the components of the second-order orientation tensor, $\Delta t = 0.1,\ T = 150$.

In the planar case, these symmetries reduce to conditions (29)–(31). The general form of (28) is given by the normalization condition [3]

$$\sum_{k=1}^{3} A_{ijkk} = A_{ij}. \tag{56}$$

Any fourth-order tensor $\mathbb{A}$ that has the symmetries $A_{ijkl} = A_{jikl} = A_{ijlk}$ can be stored in contracted form as a 6×6 matrix [17]

$$\underline{\mathbb{A}} = \begin{bmatrix} \mathbb{A}_{11} & \mathbb{A}_{12} & \mathbb{A}_{13} & \mathbb{A}_{14} & \mathbb{A}_{15} & \mathbb{A}_{16} \\ \mathbb{A}_{21} & \mathbb{A}_{22} & \mathbb{A}_{23} & \mathbb{A}_{24} & \mathbb{A}_{25} & \mathbb{A}_{26} \\ \mathbb{A}_{31} & \mathbb{A}_{32} & \mathbb{A}_{33} & \mathbb{A}_{34} & \mathbb{A}_{35} & \mathbb{A}_{36} \\ \mathbb{A}_{41} & \mathbb{A}_{42} & \mathbb{A}_{43} & \mathbb{A}_{44} & \mathbb{A}_{45} & \mathbb{A}_{46} \\ \mathbb{A}_{51} & \mathbb{A}_{52} & \mathbb{A}_{53} & \mathbb{A}_{54} & \mathbb{A}_{55} & \mathbb{A}_{56} \\ \mathbb{A}_{61} & \mathbb{A}_{62} & \mathbb{A}_{63} & \mathbb{A}_{64} & \mathbb{A}_{65} & \mathbb{A}_{66} \end{bmatrix} \tag{57}$$

with at most 36 independent components

$$\mathbb{A}_{IJ} = A_{ijkl}, \qquad I, J = 1, \ldots, 6 \tag{58}$$

where I and J are related to index pairs ij and kl as follows:

I or J	ij or kl
1	11
2	22
3	33
4	23 or 32
5	31 or 13
6	12 or 21

By symmetry of the second-order tensors $\mathbf{D}$ and $\mathbf{S} = \mathbb{A} : \mathbf{D}$, we have

$$S_{ij} = \sum_{k=1}^{3} \sum_{l=1}^{3} A_{ijkl} D_{kl} = \sum_{k=1}^{3} A_{ijkk} D_{kk} + 2 \sum_{k=1}^{3} \sum_{l=k+1}^{3} A_{ijkl} D_{kl}.$$

The contracted matrix form of this linear relationship reads [17]

$$\underline{\mathbf{S}} := \begin{bmatrix} S_{11} \\ S_{22} \\ S_{33} \\ S_{23} \\ S_{13} \\ S_{12} \end{bmatrix} = \begin{bmatrix} \mathbb{A}_{11} & \mathbb{A}_{12} & \mathbb{A}_{13} & \mathbb{A}_{14} & \mathbb{A}_{15} & \mathbb{A}_{16} \\ \mathbb{A}_{21} & \mathbb{A}_{22} & \mathbb{A}_{23} & \mathbb{A}_{24} & \mathbb{A}_{25} & \mathbb{A}_{26} \\ \mathbb{A}_{31} & \mathbb{A}_{32} & \mathbb{A}_{33} & \mathbb{A}_{34} & \mathbb{A}_{35} & \mathbb{A}_{36} \\ \mathbb{A}_{41} & \mathbb{A}_{42} & \mathbb{A}_{43} & \mathbb{A}_{44} & \mathbb{A}_{45} & \mathbb{A}_{46} \\ \mathbb{A}_{51} & \mathbb{A}_{52} & \mathbb{A}_{53} & \mathbb{A}_{54} & \mathbb{A}_{55} & \mathbb{A}_{56} \\ \mathbb{A}_{61} & \mathbb{A}_{62} & \mathbb{A}_{63} & \mathbb{A}_{64} & \mathbb{A}_{65} & \mathbb{A}_{66} \end{bmatrix} \begin{bmatrix} D_{11} \\ D_{22} \\ D_{33} \\ 2D_{23} \\ 2D_{13} \\ 2D_{12} \end{bmatrix}.$$

The remaining components of $\mathbf{S}$ are determined using the symmetry condition

$$S_{ij} = S_{ji}.$$

The transformation to the principal axes of $\mathbf{A} = \mathbf{Q}^T \hat{\mathbf{A}} \mathbf{Q}$ yields

$$\underline{\mathbb{A}} = \underline{\mathbb{M}}^T \underline{\hat{\mathbb{A}}}\, \underline{\mathbb{M}},$$

where [17]

$$\underline{\mathbb{M}} = \underline{\mathbb{F}}\,\underline{\mathbb{Q}}\,\underline{\mathbb{F}}^{-1}, \qquad \underline{\mathbb{F}} = \begin{bmatrix} 1 & 0 & 0 & 0 & 0 & 0 \\ 0 & 1 & 0 & 0 & 0 & 0 \\ 0 & 0 & 1 & 0 & 0 & 0 \\ 0 & 0 & 0 & 2 & 0 & 0 \\ 0 & 0 & 0 & 0 & 2 & 0 \\ 0 & 0 & 0 & 0 & 0 & 2 \end{bmatrix},$$

$$\underline{\mathbb{Q}} = \begin{bmatrix} Q_{11}Q_{11} & Q_{12}Q_{12} & Q_{13}Q_{13} & 2Q_{12}Q_{13} & 2Q_{11}Q_{13} & 2Q_{11}Q_{12} \\ Q_{21}Q_{21} & Q_{22}Q_{22} & Q_{23}Q_{23} & 2Q_{22}Q_{23} & 2Q_{21}Q_{23} & 2Q_{21}Q_{22} \\ Q_{31}Q_{31} & Q_{32}Q_{32} & Q_{33}Q_{33} & 2Q_{32}Q_{33} & 2Q_{31}Q_{33} & 2Q_{31}Q_{32} \\ Q_{21}Q_{31} & Q_{22}Q_{32} & Q_{23}Q_{33} & Q_{22}Q_{33}+Q_{23}Q_{32} & Q_{21}Q_{33}+Q_{23}Q_{31} & Q_{21}Q_{32}+Q_{22}Q_{31} \\ Q_{11}Q_{31} & Q_{12}Q_{32} & Q_{13}Q_{33} & Q_{12}Q_{33}+Q_{13}Q_{32} & Q_{11}Q_{33}+Q_{13}Q_{31} & Q_{11}Q_{32}+Q_{12}Q_{31} \\ Q_{11}Q_{21} & Q_{12}Q_{22} & Q_{13}Q_{23} & Q_{12}Q_{23}+Q_{13}Q_{22} & Q_{11}Q_{23}+Q_{13}Q_{21} & Q_{11}Q_{22}+Q_{12}Q_{21} \end{bmatrix}.$$

Note that the matrix $\underline{\mathbb{M}}$ of the principal axis transformation written in the contracted form is generally **not** orthogonal since $\underline{\mathbb{M}}^T = \underline{\mathbb{Q}}^{-1} \neq \underline{\mathbb{M}}^{-1}$ [17].

In view of all symmetries present in (55), the matrix $\underline{\hat{\mathbb{A}}}$ associated with an orthotropic fourth-order orientation tensor has the form [3]

$$\underline{\hat{\mathbb{A}}} = \begin{bmatrix} \hat{\mathbb{A}}_{11} & \hat{\mathbb{A}}_{12} & \hat{\mathbb{A}}_{13} & 0 & 0 & 0 \\ \hat{\mathbb{A}}_{12} & \hat{\mathbb{A}}_{22} & \hat{\mathbb{A}}_{23} & 0 & 0 & 0 \\ \hat{\mathbb{A}}_{13} & \hat{\mathbb{A}}_{23} & \hat{\mathbb{A}}_{33} & 0 & 0 & 0 \\ 0 & 0 & 0 & \hat{\mathbb{A}}_{44} & 0 & 0 \\ 0 & 0 & 0 & 0 & \hat{\mathbb{A}}_{55} & 0 \\ 0 & 0 & 0 & 0 & 0 & \hat{\mathbb{A}}_{66} \end{bmatrix} \tag{59}$$

with just nine independent nonzero components. This representation is the starting point for the derivation of orthotropic closure approximations.

4.1. Derivation of orthotropic closures

The diagonal components of the transformed second-order orientation tensor

$$\hat{\mathbf{A}} = \begin{bmatrix} \lambda_1 & 0 & 0 \\ 0 & \lambda_2 & 0 \\ 0 & 0 & \lambda_3 \end{bmatrix} = \mathbf{Q}\mathbf{A}\mathbf{Q}^T \tag{60}$$

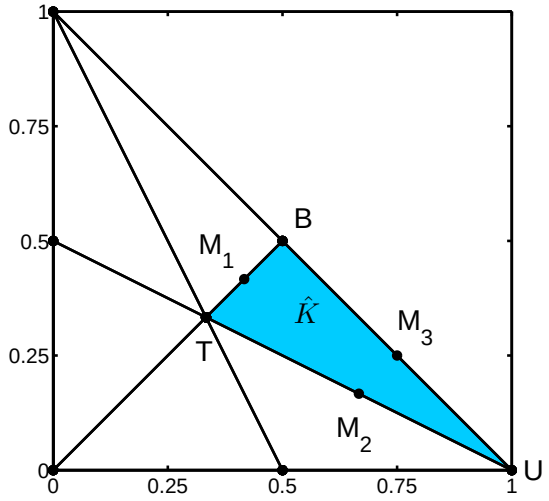

Figure 3: Reference triangle for orthotropic closures.

are nonnegative and satisfy the unit trace condition

$$\lambda_1 + \lambda_2 + \lambda_3 = 1.$$

Following Cintra and Tucker [3], we adopt the numbering convention

$$\lambda_1 \geq \lambda_2 \geq \lambda_3$$

and define the closure approximations on the triangle $\hat{K}$ formed by the principal orientation states U, B, and T as depicted in Fig. 3. Let

$$\hat{\mathbb{A}}_{11} = \hat{\mathbb{A}}_{11}(\lambda_1, \lambda_2), \tag{61}$$

$$\hat{\mathbb{A}}_{22} = \hat{\mathbb{A}}_{22}(\lambda_1, \lambda_2), \tag{62}$$

$$\hat{\mathbb{A}}_{33} = \hat{\mathbb{A}}_{33}(\lambda_1, \lambda_2) \tag{63}$$

be defined as (piecewise-)polynomial functions of λ_1 and λ_2 on $\hat{K}$. The remaining six entries of $\underline{\hat{\mathbb{A}}}$ are determined by the symmetry conditions

$$\hat{\mathbb{A}}_{12} = \hat{\mathbb{A}}_{66}, \quad \hat{\mathbb{A}}_{23} = \hat{\mathbb{A}}_{44}, \quad \hat{\mathbb{A}}_{13} = \hat{\mathbb{A}}_{55} \tag{64}$$

and the normalization conditions which can be written as [3]

$$\hat{\mathbb{A}}_{55} + \hat{\mathbb{A}}_{66} = \lambda_1 - \hat{\mathbb{A}}_{11}, \tag{65}$$

$$\hat{\mathbb{A}}_{44} + \hat{\mathbb{A}}_{66} = \lambda_2 - \hat{\mathbb{A}}_{22}, \tag{66}$$

$$\hat{\mathbb{A}}_{44} + \hat{\mathbb{A}}_{55} = \lambda_3 - \hat{\mathbb{A}}_{33}. \tag{67}$$

The edge connecting points U and B corresponds to the planar orientation state $\lambda_3 = 0$. For any point on this edge, three degrees of freedom can be determined using one of the planar closures presented in Section 3.4.

The internal point T corresponds to the triaxial isotropic orientation state

$$\lambda_1 = \lambda_2 = \lambda_3 = \frac{1}{3}, \qquad \psi(\mathbf{p}) \equiv \frac{1}{4\pi}. \tag{68}$$

At this point, the values of $\hat{\mathbb{A}}_{11},\ \hat{\mathbb{A}}_{22},\ \hat{\mathbb{A}}_{33}$ can be determined using the linear closure which is exact for isotropic orientation distributions (see below). The values of the three parameters for additional orientation states on edges TU and TB can be determined, e.g., using the exact closure relations [14] and the fact that two eigenvalues are equal on these edges (see Appendix B).

4.2. Orthotropic linear closure

The three-dimensional form of the general linear closure reads

$$\begin{aligned} A_{ijkl} = {} & \frac{1}{7}(A_{ij}\delta_{kl} + A_{ik}\delta_{jl} + A_{il}\delta_{jk} + A_{kl}\delta_{ij} + A_{jl}\delta_{ik} + A_{jk}\delta_{il}) \\ & - \frac{1}{35}(\delta_{ij}\delta_{kl} + \delta_{ik}\delta_{jl} + \delta_{il}\delta_{jk}). \end{aligned} \tag{69}$$

The values of $\hat{\mathbb{A}}_{11},\ \hat{\mathbb{A}}_{22}$, and $\hat{\mathbb{A}}_{33}$ at any point on $\hat{K}$ are given by

$$\hat{\mathbb{A}}_{11}(\lambda_1, \lambda_2) = \hat{A}_{1111}(\lambda_1, \lambda_2) = \frac{1}{7}\left(6\lambda_1 - \frac{3}{5}\right), \tag{70}$$

$$\hat{\mathbb{A}}_{22}(\lambda_1, \lambda_2) = \hat{A}_{2222}(\lambda_1, \lambda_2) = \frac{1}{7}\left(6\lambda_2 - \frac{3}{5}\right), \tag{71}$$

$$\hat{\mathbb{A}}_{33}(\lambda_1, \lambda_2) = \hat{A}_{3333}(\lambda_1, \lambda_2) = \frac{1}{7}\left(6(1 - \lambda_1 - \lambda_2) - \frac{3}{5}\right). \tag{72}$$

At the triaxial orientation point T, we have $\lambda_1 = \lambda_2 = \frac{1}{3}$. This gives

$$\hat{\mathbb{A}}_{11}(T) = \hat{\mathbb{A}}_{22}(T) = \hat{\mathbb{A}}_{33}(T) = \frac{1}{5}. \tag{73}$$

Since a one-to-one relationship between the tensors $\mathbf{A}$ and $\mathbf{B}$ is defined by formula (10), we have $\mathbf{B} = \mathbf{I}$ for the isotropic orientation distribution

$$\psi(\mathbf{p}) = \frac{1}{4\pi}\frac{1}{(\mathbf{B} : (\mathbf{p} \otimes \mathbf{p}))^{3/2}} = \frac{1}{4\pi}.$$

Substituting the eigenvalues of the unit tensor $\mathbf{B}$ into the exact closure given by equations (2.14) in [14], we find that (73) is, indeed, exact.

4.3. Orthotropic smooth closure

This closure was proposed by Cintra and Tucker [3]. It employs linear interpolation of the following parameter values at the vertices of $\hat{K}$

	U	B	T
$\hat{\mathbb{A}}_{11}$	1	$\frac{3}{8}$	$\frac{1}{5}$
$\hat{\mathbb{A}}_{22}$	0	$\frac{3}{8}$	$\frac{1}{5}$
$\hat{\mathbb{A}}_{33}$	0	0	$\frac{1}{5}$

Note that (73) is used at point T. The parameter values at points U and B are also exact. In fact, the exact closure for transversely isotropic states (see Appendix B) yields the same result as the planar natural closure:

$$\hat{\mathbb{A}}_{11}(U) = 1, \quad \hat{\mathbb{A}}_{22}(U) = \hat{\mathbb{A}}_{33}(U) = 0, \tag{74}$$

$$\hat{\mathbb{A}}_{11}(B) = \hat{\mathbb{A}}_{22}(B) = \frac{3}{8}, \quad \hat{\mathbb{A}}_{33}(B) = 0. \tag{75}$$

The coefficients of the three linear interpolation polynomials

$$\hat{\mathbb{A}}_{ii}(\lambda_1, \lambda_2) = c_{i1} + c_{i2}\lambda_1 + c_{i3}\lambda_2, \quad i = 1, 2, 3$$

can be determined by solving the linear systems

$$\begin{bmatrix} 1 & 1 & 0 \\ 1 & \frac{1}{2} & \frac{1}{2} \\ 1 & \frac{1}{3} & \frac{1}{3} \end{bmatrix} \begin{bmatrix} c_{i1} \\ c_{i2} \\ c_{i3} \end{bmatrix} = \begin{bmatrix} \hat{\mathbb{A}}_{ii}(U) \\ \hat{\mathbb{A}}_{ii}(B) \\ \hat{\mathbb{A}}_{ii}(T) \end{bmatrix}$$

or using Lagrange basis functions associated with points U, B, and T.

4.4. Orthotropic quadratic closure

An orthotropic version of the general quadratic closure

$$A_{ijkl} = A_{ij}A_{kl} \tag{76}$$

is defined by

$$\hat{\mathbb{A}}_{11}(\lambda_1, \lambda_2) = \hat{A}_{11}^2 = \lambda_1^2, \tag{77}$$

$$\hat{\mathbb{A}}_{22}(\lambda_1, \lambda_2) = \hat{A}_{22}^2 = \lambda_2^2, \tag{78}$$

$$\hat{\mathbb{A}}_{33}(\lambda_1, \lambda_2) = \hat{A}_{33}^2 = (1 - \lambda_1 - \lambda_2)^2. \tag{79}$$

This closure violates (73) but satisfies (74). The parameter values at point B are consistent with $\hat{\gamma}_1\left(\frac{1}{2}\right) = \hat{\gamma}_5\left(\frac{1}{2}\right) = \frac{1}{4}$ for the planar version (50).

4.5. Orthotropic natural closure

No analytical form of the standard natural closure [6, 16, 19] is currently known for the three-dimensional case. For this reason, we extend the planar natural closure (51) to 3D using the following reconstruction techniques.

4.5.1. Version A: extended quadratic fit

A straightforward extension of the planar natural closure to the 3D case can be constructed by fitting cubic polynomials of the form

$$\begin{aligned}\hat{\mathbb{A}}_{ii}(\lambda_1, \lambda_2) = c_{i1} + c_{i2}\lambda_1 + c_{i3}\lambda_2 + c_{i4}\lambda_1^2 + c_{i5}\lambda_1\lambda_2 \\ + c_{i6}\lambda_2^2 + c_{i7}\lambda_1\lambda_2(1 - \lambda_1 - \lambda_2)\end{aligned} \tag{80}$$

to the values of $\hat{\mathbb{A}}_{ii}$ for three uniaxial orientations corresponding to

$$U_1 = (1, 0), \quad U_2 = (0, 1), \quad U_3 = (0, 0),$$

three biaxial orientations corresponding to the edge midpoints

$$B_{12} = \left(\frac{1}{2}, \frac{1}{2}\right), \quad B_{23} = \left(0, \frac{1}{2}\right), \quad B_{31} = \left(\frac{1}{2}, 0\right),$$

and the triaxial isotropic state associated with

$$T = \left(\frac{1}{3}, \frac{1}{3}\right).$$

Using (73) and the planar natural closure (51), we obtain the data set

	U_1	U_2	U_3	B_{12}	B_{23}	B_{31}	T
$\hat{\mathbb{A}}_{11}$	1	0	0	$\frac{3}{8}$	0	$\frac{3}{8}$	$\frac{1}{5}$
$\hat{\mathbb{A}}_{22}$	0	1	0	$\frac{3}{8}$	$\frac{3}{8}$	0	$\frac{1}{5}$
$\hat{\mathbb{A}}_{33}$	0	0	1	0	$\frac{3}{8}$	$\frac{3}{8}$	$\frac{1}{5}$

In the context of numerical methods for the (Navier-)Stokes equations, the 7-node approximation (80) is known as the *extended quadratic finite element* (see [5], page 118). The incomplete set of cubic basis functions

$$\eta_i = \lambda_i(2\lambda_i - 1) + 3\lambda_1\lambda_2\lambda_3, \quad i = 1, 2, 3,$$

$$\eta_{ij} = 4\lambda_i\lambda_j - 12\lambda_1\lambda_2\lambda_3, \quad ij \in \{12, 23, 31\},$$

$$\eta_{123} = 27\lambda_1\lambda_2\lambda_3, \quad \lambda_3 = 1 - \lambda_1 - \lambda_2$$

can be used to express $\hat{\mathbb{A}}_{ii}$ in terms of the nodal values as follows:

$$\begin{aligned}\hat{\mathbb{A}}_{ii}(\lambda_1, \lambda_2) = {} & \hat{\mathbb{A}}_{ii}(U_1)\eta_1(\lambda_1, \lambda_2) + \hat{\mathbb{A}}_{ii}(U_2)\eta_2(\lambda_1, \lambda_2) + \hat{\mathbb{A}}_{ii}(U_3)\eta_3(\lambda_1, \lambda_2) \\ & + \hat{\mathbb{A}}_{ii}(B_{12})\eta_{12}(\lambda_1, \lambda_2) + \hat{\mathbb{A}}_{ii}(B_{23})\eta_{23}(\lambda_1, \lambda_2) \\ & + \hat{\mathbb{A}}_{ii}(B_{31})\eta_{31}(\lambda_1, \lambda_2) + \hat{\mathbb{A}}_{ii}(T)\eta_{123}(\lambda_1, \lambda_2). \end{aligned} \tag{81}$$

In fact, this 3D extension of the natural closure uses the same data as the orthotropic smooth closure of Cintra and Tucker [3] but interpolates this data using the extended quadratic basis on the whole triangle with vertices U_1, U_2, and U_3 instead of local linear approximation on subtriangles.

4.5.2. Version B: exact midpoint fit

Alternatively, quadratic interpolation polynomials of the form

$$\hat{\mathbb{A}}_{ii}(\lambda_1, \lambda_2) = c_{i1} + c_{i2}\lambda_1 + c_{i3}\lambda_2 + c_{i4}\lambda_1^2 + c_{i5}\lambda_1\lambda_2 + c_{i6}\lambda_2^2$$

can be constructed using the values at points U, B, T and the midpoints

$$M_1 = \left(\frac{5}{12}, \frac{5}{12}\right), \quad M_2 = \left(\frac{2}{3}, \frac{1}{6}\right), \quad M_3 = \left(\frac{3}{4}, \frac{1}{4}\right)$$

of edges BT, UT, and UB. The planar natural closure (51) yields

$$\hat{A}_{11}(M_3) = \frac{21}{32}, \quad \hat{A}_{22}(M_3) = \frac{5}{32}, \quad \hat{A}_{33}(M_3) = 0. \tag{82}$$

The same result is obtained using the three-dimensional exact closure in which the computation of **B** from **A** leads to a nonlinear system of elliptic integral relations [14]. The parameter values at points M_1 and M_2 can also be calculated using a numerical solution of this nonlinear problem or the formulae presented in Appendix B. Both approaches produce

$$\hat{\mathbb{A}}_{11}(M_1) = \hat{\mathbb{A}}_{22}(M_1) = 0.2783, \quad \hat{\mathbb{A}}_{33}(M_1) = 0.0755, \tag{83}$$

$$\hat{\mathbb{A}}_{11}(M_2) = 0.5471, \quad \hat{\mathbb{A}}_{22}(M_2) = \hat{\mathbb{A}}_{33}(M_2) = 0.0802. \tag{84}$$

In summary, the six-node quadratic interpolation employs the data set

	U	B	T	M_1	M_2	M_3
$\hat{\mathbb{A}}_{11}$	1	$\frac{3}{8}$	$\frac{1}{5}$	0.2783	0.5471	$\frac{21}{32}$
$\hat{\mathbb{A}}_{22}$	0	$\frac{3}{8}$	$\frac{1}{5}$	0.2783	0.0802	$\frac{5}{32}$
$\hat{\mathbb{A}}_{33}$	0	0	$\frac{1}{5}$	0.0755	0.0802	0

Remark. The evaluation of $\hat{A}_{11}$ defined by (81) at points M_1 and M_2 yields

$$\hat{\mathbb{A}}_{11}(M_1) = \hat{\mathbb{A}}_{22}(M_1) = 0.2778, \quad \hat{\mathbb{A}}_{33}(M_1) = 0.0799, \tag{85}$$

$$\hat{\mathbb{A}}_{11}(M_2) = 0.5444, \quad \hat{\mathbb{A}}_{22}(M_2) = \hat{\mathbb{A}}_{33}(M_2) = 0.0861. \tag{86}$$

These values are quite similar to those obtained using the exact closure.

4.6. Orthotropic mixed closure

A three-dimensional version of the planar mixed closure (52) can be constructed using piecewise-linear interpolation on four subtriangles constructed from $\hat{K}$ by connecting the midpoints M_1, M_2, M_3. In the context of finite element methods, this approximation is called P_1-iso-P_2 because it uses the same nodal points as the quadratic interpolant defined on $\hat{K}$.

The parameter values for the orthotropic mixed closure are defined by

	U	B	T	M_1	M_2	M_3	
$\hat{\mathbb{A}}_{11}$	1	$\frac{3}{8}$	$\frac{1}{5}$	$\frac{17}{60}$	$\frac{8}{15}$	$\frac{5}{8}$	
$\hat{\mathbb{A}}_{22}$	0	$\frac{3}{8}$	$\frac{1}{5}$	$\frac{17}{60}$	$\frac{1}{30}$	$\frac{1}{8}$	
$\hat{\mathbb{A}}_{33}$	0	0	$\frac{1}{5}$	$\frac{1}{30}$	$\frac{1}{30}$	0	

The values of $\hat{\mathbb{A}}_{11} = \hat{\gamma}_1$ and $\hat{\mathbb{A}}_{22} = \hat{\gamma}_5$ at M_3 are consistent with the planar mixed closure (52). Since $\hat{\mathbb{A}}_{12} = \hat{\gamma}_3 = \frac{1}{8}$ corresponds to the biaxial isotropic distribution (point B), the values of $\hat{\mathbb{A}}_{ii}$ at M_1 and M_3 are inferred from the values of $\hat{\mathbb{A}}_{12} = \hat{\mathbb{A}}_{13} = \hat{\mathbb{A}}_{23} = \frac{1}{15}$ at the triaxial isotropic state (point T).

4.7. Orthotropic fitted closures

In the below numerical study, we also consider the orthotropic fitted closure

$$\begin{bmatrix} \hat{\mathbb{A}}_{11} \\ \hat{\mathbb{A}}_{22} \\ \hat{\mathbb{A}}_{33} \end{bmatrix} = \begin{bmatrix} 0.060964 & 0.371243 & 0.555301 & -0.369160 & 0.318266 & 0.371218 \\ 0.124711 & -0.389402 & 0.258844 & 0.086169 & 0.796080 & 0.544992 \\ 1.228982 & -2.054116 & 0.821548 & -2.260574 & 1.053907 & 1.819756 \end{bmatrix} \begin{bmatrix} 1 \\ \lambda_1 \\ \lambda_1^2 \\ \lambda_2 \\ \lambda_2^2 \\ \lambda_1\lambda_2 \end{bmatrix}$$

designed by Cintra and Tucker [3] by fitting the coefficients of $\hat{\mathbb{A}}_{ii}(\lambda_1, \lambda_2)$ to numerical solutions of the Fokker-Planck equation for simple flows. In contrast to the above interpolation procedures, the data samples for this closure are not restricted to points on the boundary of triangular cells. Whereas the set of all possible orientation states can hardly be described by a single quadratic polynomial, orthotropic fitted closures of this kind belong to the most accurate general-purpose models for fiber suspension flows [4].

4.8. Numerical study of orthotropic closures

This section presents a numerical study of 3D closures for equation (5) with $\lambda_e = \frac{99}{101}$, $D_r = 0$. To calculate the probability density function ψ using (10), we evolve $\mathbf{C}$ and use it to compute $\mathbf{B} = \mathbf{C}^T\mathbf{C}$. For constant velocity gradients, the exact solution of the evolution equation (8) is given by

$$\mathbf{C}(t) = \exp\left(-t(\mathbf{W} + \lambda_e\mathbf{D})\right).$$

We remark that the use of numerical integration for calculating the second-order moment $\mathbf{A}$ of the probability density distribution $\psi(\mathbf{p})$ given by (10) can become expensive and error-prone when peaks and singularities begin to form. The associated numerical troubles could be avoided by calculating $\mathbf{A}$ and $\mathbf{B}$ using the system of evolution equations presented in [15].

The numerical approximation to $\mathbf{A}$ was advanced in time using the explicit Euler scheme and $\Delta t = 0.1$. To keep $\mathbf{A}$ positive semi-definite, we eliminate negative eigenvalues (if any) using the trace-preserving correction

$$\lambda_i := \frac{\max\{0, \lambda_i\}}{\sum_{i=1}^{3} \max\{0, \lambda_i\}}, \quad i = 1, 2, 3.$$

More advanced correction techniques can be found in [12, 13, 20, 21, 10].

The diagrams presented in Fig. 4 illustrate the evolution of the Frobenius norm error $\|\mathbf{A} - \mathbf{A}_{\text{ex}}\|_F$ for the following three-dimensional simple flows:

- Flow 1: *Uniaxial elongation*

$$\nabla \mathbf{u} = \begin{bmatrix} 0.02 & 0.0 & 0.0 \\ 0.0 & -0.01 & 0.0 \\ 0.0 & 0.0 & -0.01 \end{bmatrix}.$$

- Flow 2: *Biaxial elongation*

$$\nabla \mathbf{u} = \begin{bmatrix} 0.01 & 0.0 & 0.0 \\ 0.0 & 0.01 & 0.0 \\ 0.0 & 0.0 & -0.02 \end{bmatrix}.$$

- Flow 3: *Simple shear*

$$\nabla \mathbf{u} = \begin{bmatrix} 0.0 & 0.05 & 0.0 \\ 0.0 & 0.0 & 0.0 \\ 0.0 & 0.0 & 0.0 \end{bmatrix}.$$

- Flow 4: *Shearing and stretching*

$$\nabla \mathbf{u} = \begin{bmatrix} -0.01 & 0.01 & 0.0 \\ 0.0 & -0.01 & 0.0 \\ 0.0 & 0.0 & 0.02 \end{bmatrix}.$$

The initial conditions for the first test are given by the isotropic orientation state at point T. Uniaxial elongation corresponds to moving from this point toward point U along edge TU. Biaxial elongation corresponds to moving

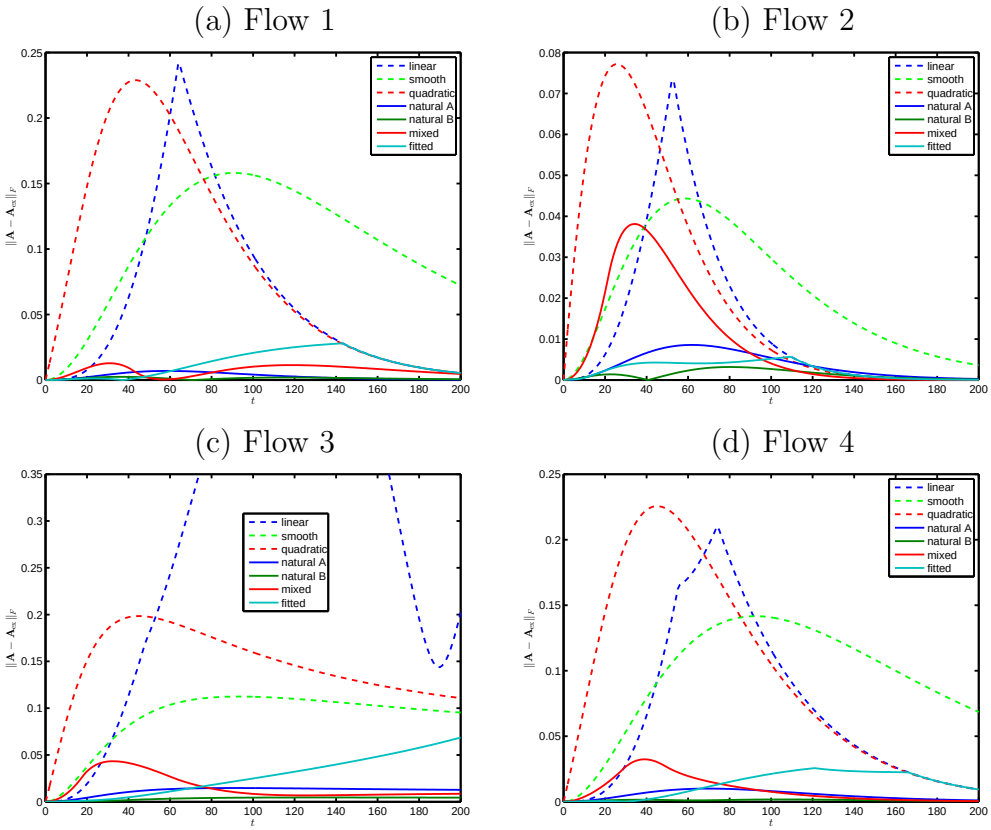

Figure 4: Numerical study of orthotropic closures: Frobenius norm of the error in the components of the second-order orientation tensor, $\Delta t = 0.1$, $\mathbf{A}(0) = \text{diag}\left\{\frac{1}{3}, \frac{1}{3}, \frac{1}{3}\right\}$.

from point T toward point B along edge TB. A sketch of trajectories corresponding to both types of shearing flows can be found in [3].

The linear closure was found to require frequent correction of negative eigenvalues, as shown in Fig. 5. At the time instants when the smallest eigenvalue of $\mathbf{A}$ becomes negative and the eigenvalue correction procedure is activated, the error stops growing and begins to decrease. Occasional eigenvalue corrections were also required by the orthotropic fitted closure, whereas other closures did not produce negative eigenvalues in this experiment.

The labels A and B in the legends of Fig. 4 refer to orthotropic natural closures based on the extended quadratic interpolation (81) and standard quadratic interpolation for exact midpoint values (83),(84), respectively. It

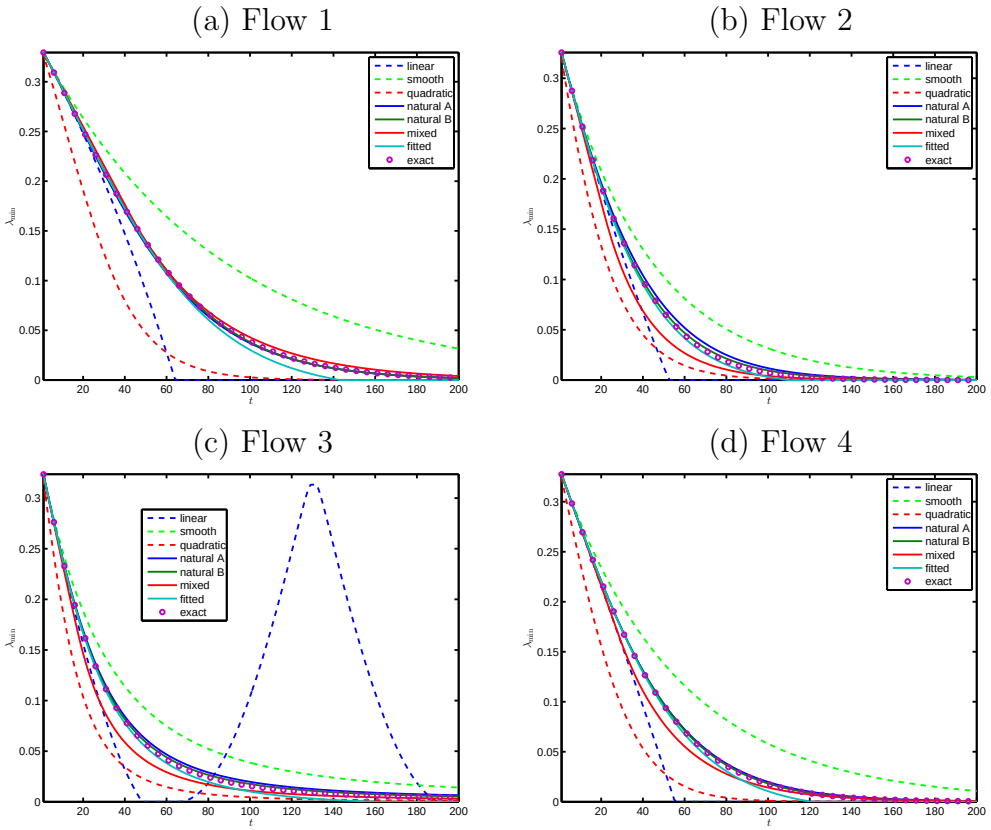

Figure 5: Evolution of the smallest eigenvalue of $\mathbf{A}$ computed using orthotropic closures with elimination of negative eigenvalues, $\mathbf{A}(0) = \operatorname{diag}\left\{\frac{1}{3}, \frac{1}{3}, \frac{1}{3}\right\}$.

can be seen that version B produces the best results for isotropic initial conditions. Version A also performs remarkably well. For times $t \leq 100$ the piecewise-linear mixed closure tends to be less accurate than the natural and fitted closures but more accurate than the linear, quadratic, and smooth closures. In the long run, it becomes more accurate than the fitted closure and even more accurate than natural closure A for Flows 2-4.

To assess the ability of the presented closures to handle arbitrary initial conditions, we perform the same comparative study using

$$\mathbf{A}(0) = \begin{bmatrix} 0.25 & 0 & 0 \\ 0 & 0.35 & 0 \\ 0 & 0 & 0.4 \end{bmatrix}.$$

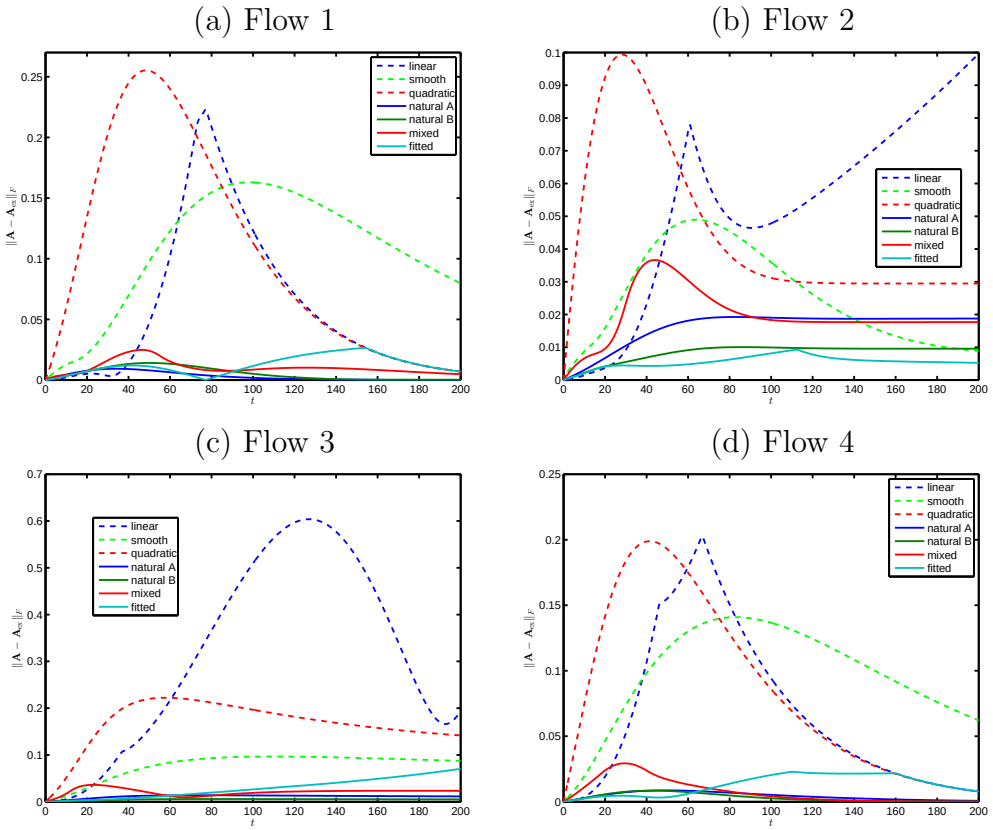

Figure 6: Numerical study of orthotropic closures: Frobenius norm of the error in the components of the second-order orientation tensor, $\Delta t = 0.1$, $\mathbf{A}(0) = \text{diag}\{0.25, 0.35, 0.4\}$.

The initial condition ψ_0 for the exact solution defined by (7) is computed from $\mathbf{A}(0)$ using the orientation distribution reconstruction functions presented in [8]. The general formula for a second-order reconstruction $\hat{\psi}$ reads

$$\hat{\psi}(\mathbf{p}) = \frac{1}{4\pi}\left[1 + \frac{15}{2}\sum_{i,j=1}^{3}\left(A_{ij} - \frac{1}{3}\delta_{ij}\right)\left(p_i p_k - \frac{1}{3}\delta_{ij}\right)\right].$$

Since $\mathbf{A}(0)$ is diagonal in our test, the formula for ψ_0 simplifies to

$$\psi_0(\mathbf{p}) = \frac{1}{4\pi}\left[1 + \frac{15}{2}\sum_{i}^{3}\left(A_{ii}(0) - \frac{1}{3}\right)\left(p_i^2 - \frac{1}{3}\right)\right].$$

It is easy to verify that the second moment of ψ_0 is equal to $\mathbf{A}(0)$.

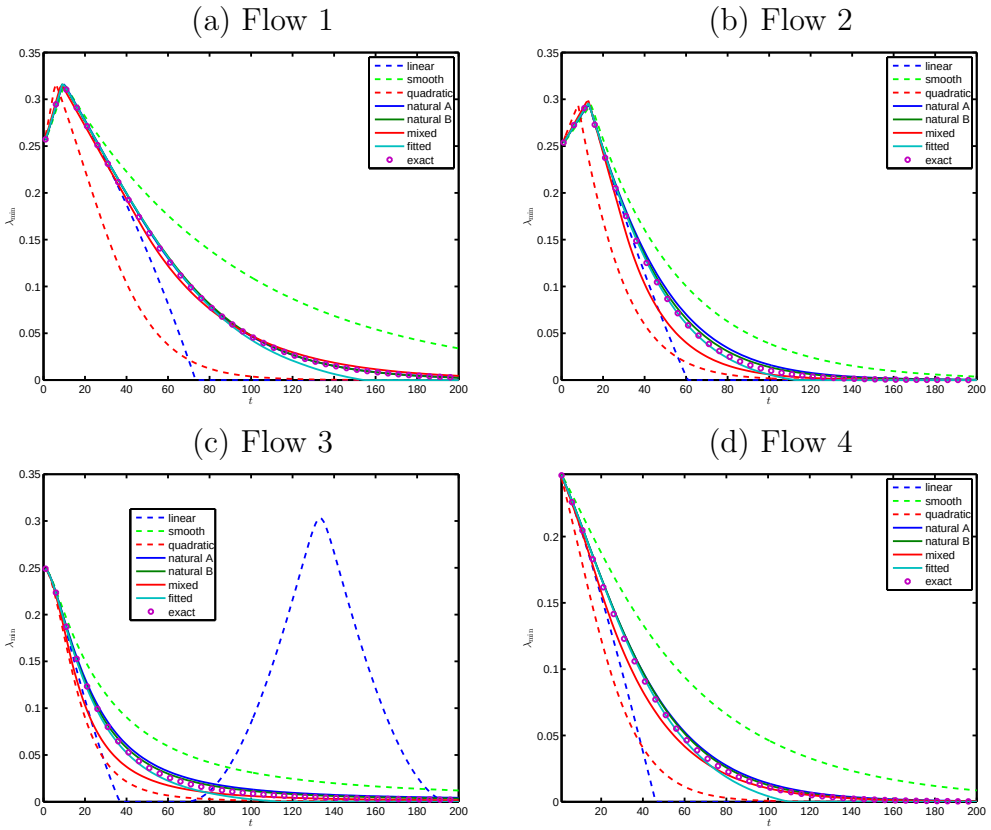

Figure 7: Evolution of the smallest eigenvalue of $\mathbf{A}$ computed using orthotropic closures with elimination of negative eigenvalues, $\mathbf{A}(0) = \mathrm{diag}\,\{0.25, 0.35, 0.4\}$.

The results presented in Figs 6 and 7 demonstrate that the natural and mixed closures remain more accurate than other closures for Flows 1, 3, and 4. The best results for Flow 2 are produced by the fitted closure. The stagnation of some error curves in Fig. 6(b) can be attributed to the fact that direct calculation of the exact second-order moment $\mathbf{A}_{\mathrm{ex}}$ from the exact probability density (7) cannot be performed with desired precision due to formation of singularities at early stages of the simulation run. Due to the lack of a sufficiently accurate reference solution, no final conclusions regarding the accuracy of different closures can be drawn in this case. For instance, the error curve of the smooth closure in Fig. 6(b) indicates that it eventually becomes more accurate than most other closures but Fig. 7(b) reveals that other closures do a better job in predicting the smallest eigenvalue of $\mathbf{A}$.

5. Summary

The presented work indicates that a detailed investigation of 2D orientation dynamics is a useful exercise which leads to a better understanding of existing relationships and simple 3D extensions of closed-form expressions derived for the planar case. The adopted design philosophy is based on using exact formulas or asymptotic expansions for orientation dynamics under certain ideal conditions (such as planar, aligned, biaxial isotropic, or fully isotropic states) to generate data sets for polynomial fitting in the principal axis system. More accurate closures can be constructed using finite element interpolation on a mesh of subcells. The orientation states at additional nodal points can be recovered, e.g., using the exact closure as in version B of our orthotropic natural closure. We also envisage that the dependence of orientation patterns on the rotary diffusion coefficient can be taken into account.

Acknowledgments

The author would like to thank Christoph Lohmann (TU Dortmund University), Prof. Oleg Iliev (Fraunhofer Institute for Industrial Mathematics, Kaiserslautern), and Prof. Alexander Panchenko (Washington State University) for inspiring discussions on fiber orientation modeling.

This research was supported by the German Research Association (DFG) under grant KU 1530/13-1.

References

[1] S.G. Advani and C.L. Tucker, The use of tensors to describe and predict fiber orientation in short fiber composites. *J. Rheol.* **31** (1987) 751–784.

[2] M.C. Altan and L. Tang, Orientation tensors in simple flows of dilute suspensions of non-Brownian rigid ellipsoids, comparison of analytical and approximate solutions. *Rheol. Acta* **32** (1993) 227-244.

[3] J.S. Cintra and C.L. Tucker III, Orthotropic closure approximations for flow-induced fiber orientation. *J. Rheol.* **39** (1995) 1095–1121.

[4] D.H. Chung and T.H. Kwon, Improved model of orthotropic closure approximation for flow induced fiber orientation, *Polymer Composites* **22** (2001) 636-649.

[5] C. Cuvelier, A. Segal, A.A. van Steenhoven, *Finite Element Methods and Navier-Stokes Equations*. Kluwer, 1986.

[6] F. Dupret and V. Verleye, Modelling the flow of fiber suspensions in narrow gaps. *Advances in the Flow and Rheology of Non-Newtonian Fluids* **8** (1999) 1347–1398.

[7] F.P. Folgar and C.L. Tucker, Orientation behavior of fibers in concentrated suspensions. *Journal of Reinforced Plastics and Composites* **3** (1984) 98–119.

[8] D.A. Jack and D.E. Smith, Assessing the use of tensor closure methods with orientation distribution reconstruction functions. *Journal of Composite Materials* **38** (2004) 1851–1871.

[9] G.B. Jeffery, The motion of ellipsoidal particles immersed in a viscous fluid. *Proc. Roy. Soc. Lon* **A102** (1922) 161–179.

[10] D.S. Kershaw, Flux limiting nature's own way – A new method for numerical solution of the transport equation. Lawrence Livermore National Laboratory, 1976.

[11] G.G. Lipscomb II, M.M. Denn, D.U. Hur, D.V. Boger, The flow of fiber suspensions in complex geometries. *Journal of Non-Newtonian Fluid Mechanics* **26** (1998) 297–325.

[12] C. Lohmann, Galerkin-Spektralverfahren für die Fokker-Planck-Gleichung (*Galerkin Spectral Methods for the Fokker-Planck Equation*, in German). Springer Spektrum: BestMasters, 2016.

[13] C. Lohmann, Efficient algorithms for constraining orientation tensors in Galerkin methods for the Fokker-Planck equation. *Computers & Mathematics with Applications* **71** (2016) 1059–1073.

[14] S. Montgomery-Smith, W. He, D. A. Jack, D. E. Smith, Exact tensor closures for the three-dimensional Jeffery's equation. *J. Fluid Mech.* **680** (2011) 321–335.

[15] S. Montgomery-Smith, D. Jack, D. E. Smith, The fast exact closure for Jefferys equation with diffusion. *Journal of Non-Newtonian Fluid Mechanics*, **166** (2011) 343–353.

[16] E. Pruliére, A. Ammar, F. Chinesta, Empirical natural closure relation for short fiber suspension models. *International Journal of Forming Processes* **10** (2007) 1292–7775.

[17] M.A. Slawinski, *Waves and Rays in Elastic Continua*. World Scientific, second edition, 2007.

[18] A.J. Szeri and D.J. Lin, A deformation tensor model of Brownian suspensions of orientable particles – the nonlinear dynamics of closure models. *Journal of Non-Newtonian Fluid Mechanics* **64** (1996) 43–69.

[19] V. Verleye and F. Dupret, Prediction of fiber orientation in complex injection molded parts. In: D. A. Siginer (Ed.), *Developments in Non-Newtonian Flows*, AMD-Vol. **175**, ASME 1993, pp. 139–163.

[20] B.E. VerWeyst, *Numerical Predictions of Flow-Induced Fiber Orientation in Three-Dimensional Geometries*. PhD thesis, University of Illinois, 1998.

[21] B.E. VerWeyst and C.L. Tucker III, Fiber suspensions in complex geometries: Flow/orientation coupling. *Canadian J. Chem. Eng.* **80** (2002) 1093–1106.

Appendix A: Natural closure in 2D

In the planar case $d = 2$, equations (10)–(12) of the exact closure become

$$\psi(\mathbf{p}) = \frac{1}{2\pi} \frac{1}{\mathbf{B} : (\mathbf{p} \otimes \mathbf{p})}, \qquad \mathbf{p} = \begin{bmatrix} \cos\varphi \\ \sin\varphi \end{bmatrix},$$

$$\mathbf{A} = \frac{1}{2\pi} \int_0^{2\pi} \frac{\mathbf{p} \otimes \mathbf{p}}{\mathbf{B} : (\mathbf{p} \otimes \mathbf{p})} \, \mathrm{d}\varphi,$$

$$\mathbb{A} = \frac{1}{2\pi} \int_0^{2\pi} \frac{\mathbf{p} \otimes \mathbf{p} \otimes \mathbf{p} \otimes \mathbf{p}}{\mathbf{B} : (\mathbf{p} \otimes \mathbf{p})} \, \mathrm{d}\varphi.$$

Since $\mathbf{A}$ and $\mathbf{B}$ are simultaneously diagonalizable, we have

$$\hat{\mathbf{A}} = \begin{bmatrix} \lambda_1 & 0 \\ 0 & \lambda_2 \end{bmatrix} = \begin{bmatrix} \lambda & 0 \\ 0 & 1-\lambda \end{bmatrix} = \mathbf{Q}\mathbf{A}\mathbf{Q}^T,$$

$$\hat{\mathbf{B}} = \begin{bmatrix} \mu_1 & 0 \\ 0 & \mu_2 \end{bmatrix} = \begin{bmatrix} \mu & 0 \\ 0 & \frac{1}{\mu} \end{bmatrix} = \mathbf{Q}\mathbf{B}\mathbf{Q}^T,$$

$$\hat{\mathbf{B}} : (\mathbf{p} \otimes \mathbf{p}) = \mathbf{p} \cdot \hat{\mathbf{B}}\mathbf{p} = \mu \cos^2\varphi + \frac{1}{\mu}\sin^2\varphi.$$

Calculating the integral

$$\hat{A}_{11} = \frac{1}{2\pi}\int_0^{2\pi} \frac{\cos^2\varphi}{\mu\cos^2\varphi + \frac{1}{\mu}\sin^2\varphi}\,\mathrm{d}\varphi = \lambda,$$

one obtains

$$\lambda = \frac{1}{1+\mu}, \qquad 1-\lambda = \frac{\mu}{1+\mu},$$
$$\mu = \frac{1-\lambda}{\lambda}, \qquad \frac{1}{\mu} = \frac{\lambda}{1-\lambda}.$$

It follows that

$$\begin{aligned} \hat{\mathbf{B}} : (\mathbf{p} \otimes \mathbf{p}) &= \frac{1-\lambda}{\lambda}\cos^2\varphi + \frac{\lambda}{1-\lambda}\sin^2\varphi \\ &= \frac{\lambda^2\sin^2\varphi + (1-\lambda)^2\cos^2\varphi}{\lambda(1-\lambda)}, \end{aligned}$$

whence

$$\hat{A}_{ijkl} = \frac{1}{2\pi}\int_0^{2\pi} \frac{\cos^m\varphi\sin^n\varphi\lambda(1-\lambda)}{\lambda^2\sin^2\varphi + (1-\lambda)^2\cos^2\varphi}\,\mathrm{d}\varphi, \quad m+n=4,$$
$$m = \delta_{i1}+\delta_{j1}+\delta_{k1}+\delta_{l1}, \quad n = \delta_{i2}+\delta_{j2}+\delta_{k2}+\delta_{l2}.$$

Thus the matrix form (42) of $\hat{\mathbb{A}}$ is defined by (cf. [19])

$$\hat{\gamma}_1(\lambda) = \frac{1}{2}\lambda(1+\lambda),$$
$$\hat{\gamma}_3(\lambda) = \frac{1}{2}\lambda(1-\lambda),$$
$$\hat{\gamma}_5(\lambda) = \frac{1}{2}(1-\lambda)(2-\lambda),$$

as in the planar natural closure presented in Section 3.4. This proves that the natural closure is exact for $D_r = 0$ under the assumption that the isotropic orientation state occurs at some point in evolution history.

Appendix B: Natural closure in 3D

No analytical form of the natural closure is known for the 3D case in which

$$\psi(\mathbf{p}) = \frac{1}{4\pi}\frac{1}{(\mathbf{B}:(\mathbf{p}\otimes\mathbf{p}))^{3/2}}, \qquad \mathbf{p} = \begin{bmatrix} \sin\theta\cos\varphi \\ \sin\theta\sin\varphi \\ \cos\theta \end{bmatrix},$$

$$\mathbf{A} = \frac{1}{4\pi}\int_0^{2\pi}\int_0^{\pi} \frac{\mathbf{p}\otimes\mathbf{p}}{(\mathbf{B}:(\mathbf{p}\otimes\mathbf{p}))^{3/2}}\sin\theta\,\mathrm{d}\theta\mathrm{d}\varphi,$$

$$\mathbb{A} = \frac{1}{4\pi}\int_0^{2\pi}\int_0^{\pi} \frac{\mathbf{p}\otimes\mathbf{p}\otimes\mathbf{p}\otimes\mathbf{p}}{(\mathbf{B}:(\mathbf{p}\otimes\mathbf{p}))^{3/2}}\sin\theta\,\mathrm{d}\theta\mathrm{d}\varphi.$$

However, some simplifications are possible if two eigenvalues of $\mathbf{A}$ coincide, i.e., for transversely isotropic states corresponding to edges TU and BU of $\hat{K}$ in Fig. 3. In the case $\lambda_1 = \lambda_2$, the principal axis transformation yields

$$\hat{\mathbf{A}} = \begin{bmatrix} \lambda_1 & 0 & 0 \\ 0 & \lambda_2 & 0 \\ 0 & 0 & \lambda_3 \end{bmatrix} \begin{bmatrix} \lambda & 0 & 0 \\ 0 & \lambda & 0 \\ 0 & 0 & 1-2\lambda \end{bmatrix} = \mathbf{Q}\mathbf{A}\mathbf{Q}^T.$$

Since the relationship between $\hat{\mathbf{A}}$ and $\hat{\mathbf{B}}$ is one-to-one and defined by equations (2.8) in [14], the first two eigenvalues of $\mathbf{B}$ must also be equal. Thus

$$\hat{\mathbf{B}} = \begin{bmatrix} \mu_1 & 0 & 0 \\ 0 & \mu_2 & 0 \\ 0 & 0 & \mu_3 \end{bmatrix} = \begin{bmatrix} \mu & 0 & 0 \\ 0 & \mu & 0 \\ 0 & 0 & \frac{1}{\mu^2} \end{bmatrix} = \mathbf{Q}\mathbf{B}\mathbf{Q}^T,$$

$$\hat{\mathbf{B}}\mathbf{p} = \left[\mu\sin\theta\cos\varphi, \mu\sin\theta\sin\varphi, \frac{1}{\mu^2}\cos\theta\right]^T,$$

$$\hat{\mathbf{B}}:(\mathbf{p}\otimes\mathbf{p}) = \mu\sin^2\theta + \frac{1}{\mu^2}\cos^2\theta,$$

where μ is the unique solution to the nonlinear problem

$$\lambda = \hat{A}_{11} = \frac{1}{4\pi}\int_0^{2\pi}\int_0^{\pi} \frac{\sin^3\theta\cos^2\varphi}{\left(\mu\sin^2\theta + \frac{1}{\mu^2}\cos^2\theta\right)^{3/2}}\,\mathrm{d}\theta\,\mathrm{d}\varphi,$$

$$= \frac{1}{4}\int_0^{\pi} \frac{\sin^3\theta}{\left(\mu\sin^2\theta + \frac{1}{\mu^2}\cos^2\theta\right)^{3/2}}\,\mathrm{d}\theta.$$

This problem can be solved numerically for any value of $\lambda \in [0,1]$ and the resulting numerical solution $\mu = \mu(\lambda)$ can be used to compute

$$\begin{aligned}\hat{\mathbb{A}}_{11} = \hat{A}_{1111} &= \frac{1}{4\pi}\int_0^{2\pi}\int_0^{\pi} \frac{\sin^5\theta\cos^4\varphi}{\left(\mu\sin^2\theta + \frac{1}{\mu^2}\cos^2\theta\right)^{3/2}}\,\mathrm{d}\theta\mathrm{d}\varphi,\\ &= \frac{3}{16}\int_0^{\pi} \frac{\sin^5\theta}{\left(\mu\sin^2\theta + \frac{1}{\mu^2}\cos^2\theta\right)^{3/2}}\,\mathrm{d}\theta,\end{aligned}$$

$$\begin{aligned}\hat{\mathbb{A}}_{22} = \hat{A}_{2222} &= \frac{1}{4\pi}\int_0^{2\pi}\int_0^{\pi} \frac{\sin^5\theta\sin^4\varphi}{\left(\mu\sin^2\theta + \frac{1}{\mu^2}\cos^2\theta\right)^{3/2}}\,\mathrm{d}\theta\mathrm{d}\varphi,\\ &= \frac{3}{16}\int_0^{\pi} \frac{\sin^5\theta}{\left(\mu\sin^2\theta + \frac{1}{\mu^2}\cos^2\theta\right)^{3/2}}\,\mathrm{d}\theta,\end{aligned}$$

$$\begin{aligned}\hat{\mathbb{A}}_{33} = \hat{A}_{3333} &= \frac{1}{4\pi}\int_0^{2\pi}\int_0^{\pi} \frac{\sin\theta\cos^4\theta}{\left(\mu\sin^2\theta + \frac{1}{\mu^2}\cos^2\theta\right)^{3/2}}\,\mathrm{d}\theta\mathrm{d}\varphi\\ &= \frac{1}{2}\int_0^{\pi} \frac{\sin\theta\cos^4\theta}{\left(\mu\sin^2\theta + \frac{1}{\mu^2}\cos^2\theta\right)^{3/2}}\,\mathrm{d}\theta.\end{aligned}$$